FEDERAL SCIENCE POLICY OFFICE

PROGRAMME FOR EARTH OBSERVATION

AQUASCOPE

ALGORITHM THEORETICAL BASELINE DOCUMENT

CONTRACT CB/36/15

AQUASCOPE

Integration of a EO data service for North Sea users with aquatic products within the Terrascope framework

Date: 03/11/2026

For the partnership: RBINS (Dimitry Van der Zande) – VITO (Jurgen Everaerts)

Contributors

- Dimitry Van der Zande (RBINS)
- Arthur Coqué (RBINS)

Change record

Issue	Date	§	Description of Change	Author	Validated By
1.00	28.02.2026	All	Initial version of the document	D. Van der Zande, A. Coqué, Q. Vanhellemont	
1.01	03.11.2026	DVDZ, AC	Revision of document	D. Van der Zande	A. Coqué

CONTENT

Contributors 1

Change record 2

CONTENT 2

1 EXECUTIVE SUMMARY 4

1.1 Products covered by this document 4

1.2 Summary of the results 6

1.3 Estimated Accuracy Numbers 7

2 PRODUCTION SYSTEM DESCRIPTION 8

2.1 Production centre: RBINS and VITO 8

2.2 AQUASCOPE production system 8

2.3 INput products 10

3 PROCESSING STEPS 11

3.1 Pixel classification 12

3.2 Atmospheric correction 13

3.3 Suspended Particulate matter (SPM) and turbidity (TUR) 19

3.4 Chlorophyll-a concentration (CHL) 21

3.5 Sea Surface temperature (SST) 24

3.6 RGB imagery 26
4 TEMPORAL COVERAGE 27
4.1 temporal aggregation 27
5 VALIDATION FRAMEWORK 27
5.1 Radiometric in situ data 27
5.2 Biogeochemical in situ data 28
6 OFFLINE VALIDATION 29
6.1 Matchup analysis and statistical measures 29
6.2 Remote sensing reflectance (RRS) 30
6.3 Chlorophyll-a concentration (CHL) 33
6.4 Suspended particulate matter (SPM) 35
6.5 Sea surface temperature (SST) 38
7 SYSTEM'S NOTICEABLE EVENTS, OUTAGES OR CHANGES 40
8 REFERENCES 40

1 EXECUTIVE SUMMARY

1.1 PRODUCTS COVERED BY THIS DOCUMENT

The AQUASCOPE service provides aquatic Earth Observation products for the Belgian North Sea within the Terrascope framework. Daily, monthly, and yearly products are provided based on Sentinel-2/MSI, Sentinel-3/OLCI, Sentinel-3/SLSTR, and Landsat-8/9 data. The AQUASCOPE products include:

OPTICS PRODUCTS

- **Remote Sensing Reflectance (RRS)**

  The Remote Sensing Reflectance (RRS) product is the spectral reflectance of the water surface after atmospheric correction of the satellite Level-1 data, expressed as remote sensing reflectance in units of sr^{-1}. It represents the ratio between the water-leaving radiance and the downwelling solar irradiance just above the sea surface, and is the fundamental optical product from which all other ocean colour variables in AQUASCOPE (e.g. SPM, TUR, CHL) are derived.

BIOGEOPHYSICAL PRODUCTS

- **Suspended Particulate Matter (SPM)**
- *Suspended Particulate Matter (SPM), also called total suspended matter (TSM; Nechad et al., 2010), is the dry mass concentration of all particles in the near-surface water that are retained on a glass-fiber filter (GF/F): mineral sediments, organic detritus and living phytoplankton. It is measured gravimetrically on pre-washed GF/F filters (Tilstone et al., 2003; van der Linde, 1998) and expressed in g m^{-3} (equivalent to mg L^{-1}). It is a key water-quality indicator controlling water clarity and light penetration. The satellite SPM is retrieved with the single-band algorithm of Nechad et al. (2010), applied to a red (665 nm) and a near-infrared (865 nm) band; the two retrievals are merged with the band-switching approach of Novoa et al. (2017), which uses the red band in low to moderately turbid waters and the near-infrared band in very turbid waters, where the red reflectance saturates (section 3.3). The Nechad et al. (2010) algorithm is less appropriate in low-SPM, phytoplankton-dominated waters; a detection limit of 1 g m^{-3} is suggested for this method.*
- **Turbidity (TUR)**
- *Turbidity (TUR) is an optical property of water that quantifies the scattering of light by suspended particles (mineral sediments, organic detritus and phytoplankton), with higher turbidity indicating cloudier water. Following ISO 7027 (ISO, 1999), it is measured with a nephelometer as the ratio of the light scattered at 90° to the light transmitted forward at 860 nm, relative to the same ratio for a Formazin standard suspension, and is expressed in Formazin Nephelometric Units (FNU) (Nechad et al., 2009). The near-infrared wavelength minimises the influence of light absorption by particles and coloured dissolved*

organic matter. Turbidity is closely correlated with SPM but, as an optical property, it does not depend on the mass density of the particles. It is a key water-quality indicator, listed in the EU Marine Strategy Framework Directive. The satellite TUR is retrieved from the red (665 nm) and near-infrared (865 nm) reflectances with the algorithm of Nechad et al. (2009); as for SPM, the two retrievals are merged with the band-switching approach of Novoa et al. (2017) (section 3.3).

- **Chlorophyll-a concentration (CHL)**

  Chlorophyll-a concentration (CHL) is the mass concentration of the phytoplankton pigment chlorophyll-a in the near-surface water, expressed in mg m^{-3} (equivalent to µg L^{-1}). Chlorophyll-a is present in all phytoplankton and is used as a proxy for phytoplankton biomass. It is a core indicator for monitoring blooms, eutrophication status and marine ecosystem productivity, used in the OSPAR eutrophication assessment and the EU Marine Strategy Framework Directive. The in situ reference is measured on filtered water samples: the pigments retained on the filter are extracted and chlorophyll-a is quantified by high-performance liquid chromatography (HPLC). The satellite CHL is retrieved from the remote sensing reflectance with OCTIS, which reproduces the Copernicus Marine multi-algorithm CHL (Lavigne et al., 2021) recalibrated to in situ HPLC data.

THERMAL PRODUCTS

- **Sea Surface Temperature (SST)**

  Sea Surface Temperature (SST) is the temperature of the sea water at the surface, expressed in kelvin or degrees Celsius. The AQUASCOPE SST is the skin temperature retrieved from thermal-infrared radiances after atmospheric correction: Sentinel-3/SLSTR Level-2 WST products (1 km) and Landsat-8/9/TIRS Collection-2 Level-2 Surface Temperature products (30 m). SST is a key variable for monitoring marine heatwaves, air–sea heat exchange, fronts, ocean circulation and ecosystem responses.

ADDITIONAL PRODUCTS

- **RGB imagery**

  RGB imagery is a quasi–true-colour product that combines three visible-band reflectance channels into red, green and blue display channels to create a natural-looking image of the sea surface, similar to what the human eye would see from space. In AQUASCOPE, RGB maps are built from remote sensing reflectance bands in the blue, green and red (e.g. Rrs490, Rrs560, Rrs665), and are mainly used for intuitive visual inspection and feature detection (fronts, foam lines, blooms, ship wakes, slicks, etc.).

1.2 SUMMARY OF THE RESULTS

Estimated Accuracy Numbers (EANs) give a quick overview of the performance of the AQUASCOPE products with respect to *in situ* observations (Table 1); the full analysis is given in section 6. The RRS is validated against the HYPERNETS radiometers at Oostende and Thornton Bank (2020–2025), the CHL against the HPLC data of Rijkswaterstaat in the Dutch coastal waters (2019–2025), the SPM against the monitoring campaigns of RBINS with the research vessel Belgica (2018–2023) and the SST against the Meetnet Vlaamse Banken (April 2025 – March 2026). The TUR products have not yet been validated against *in situ* data; as they are retrieved with the same algorithm and bands as the SPM, they are expected to have similar uncertainty characteristics, without the additional uncertainty of the conversion from optical properties to particle mass.

Remote sensing reflectance: for all three sensors, the merged RRS agrees better with the *in situ* data than ACOLITE or C2RCC alone, with an RMSD of 0.0028–0.0033 sr^{-1}, a MAPD of 18–22% and a bias close to zero over all bands. The merge cancels the opposite biases of ACOLITE (overestimation) and C2RCC (underestimation). The relative differences are smallest in the visible bands (MAPD 12–24%) and larger in the red-edge and near-infrared bands (30–42%), where the reflectance itself is small.

Chlorophyll-a: the OCTIS CHL follows the 1:1 line from 0.1 to 50 mg m^{-3} with a small positive bias (+0.02 for Sentinel-3, +0.05 for Sentinel-2, log10), an RMSD of 0.31–0.32 (log10) and a MAPD of 42% (Sentinel-3) and 49% (Sentinel-2). At the same matchups it agrees better with the *in situ* data than the CMEMS multi-sensor 1 km and HR-OC 100 m CHL products.

Suspended particulate matter: the satellite SPM follows the *in situ* SPM over two orders of magnitude, from about 3 to more than 100 g m^{-3} (r^2 = 0.78 for Sentinel-3 and 0.88 for Sentinel-2, log10), but underestimates it, with a median ratio satellite/*in situ* of 0.62 (Sentinel-3) and 0.38 (Sentinel-2). The underestimation is largest at the offshore stations with low SPM (3–7 g m^{-3}); its cause is under investigation. The results rest on 32 (Sentinel-3) and 11 (Sentinel-2) matchups.

Sea surface temperature: both sensors agree closely with the *in situ* temperature over the seasonal range of 4 to 22 °C: RMSD 0.72 °C and bias −0.33 °C for Sentinel-3/SLSTR, RMSD 0.85 °C and bias −0.09 °C for Landsat-8/9/TIRS. Four Landsat overpasses affected by undetected clouds or cloud shadows (3 to 5 °C too cold) are excluded. The satellite SST is slightly lower than the *in situ* temperature in spring and summer and slightly higher in autumn and winter.

1.3 ESTIMATED ACCURACY NUMBERS

Table 1 summarises the Estimated Accuracy Numbers of the AQUASCOPE L3D products, computed with the metrics of Table 6 (section 6.1).

Table 1: Estimated Accuracy Numbers of the AQUASCOPE L3D products (metrics of Table 6). RRS: all bands together, N = matchups (spectra × bands); CHL and SPM: slope, r^2, RMSD and bias on log10, MAPD on the concentration; SST: in °C, MAPD not used, Landsat without the four cloud-affected overpasses. S: type-2 slope, r^2: coefficient of determination, RMSD: root mean square difference, MAPD: median absolute percentage difference, N: number of matchups.

Product	Sensor	*In situ* reference	Units	S	r^2	RMSD	Bias	MAPD (%)	N
RRS	Sentinel-3/OLCI	HYPERNETS	sr^{-1}	0.92	0.87	0.0032	−0.0006	22	197 (2758)
RRS	Sentinel-2/MSI	HYPERNETS	sr^{-1}	0.98	0.92	0.0028	+0.0001	20	118 (944)
RRS	Landsat-8/9/OLI	HYPERNETS	sr^{-1}	0.91	0.91	0.0033	−0.0002	18	42 (210)
CHL	Sentinel-3/OLCI	RWS (HPLC)	log10(mg m^{-3})	0.95	0.66	0.31	+0.02	42	255
CHL	Sentinel-2/MSI	RWS (HPLC)	log10(mg m^{-3})	0.92	0.52	0.32	+0.05	49	96
SPM	Sentinel-3/OLCI	RBINS (Belgica)	log10(g m^{-3})	1.07	0.78	0.37	−0.24	45	32
SPM	Sentinel-2/MSI	RBINS (Belgica)	log10(g m^{-3})	1.18	0.88	0.43	−0.35	69	11
TUR	Sentinel-3/OLCI, Sentinel-2/MSI	not yet validated	FNU	–	–	–	–	–	–
SST	Sentinel-3/SLSTR	Meetnet Vlaamse Banken	°C	0.92	0.99	0.72	−0.33	–	55
SST	Landsat-8/9/TIRS	Meetnet Vlaamse Banken	°C	0.94	0.98	0.85	−0.09	–	24

2 PRODUCTION SYSTEM DESCRIPTION

2.1 PRODUCTION CENTRE: RBINS AND VITO

RBINS (Royal Belgian Institute of Natural Sciences) - Algorithm Development and Validation:

- Algorithm development and optimization for Belgian coastal waters
- Product validation using *in situ* measurements
- Quality control and user support
- Service desk operations

VITO (Flemish Institute for Technological Research) - Terrascope Infrastructure:

- Satellite data archive access
- Cloud computing processing capacity
- Web viewer interface for data visualization
- EOPlaza for customized product generation

2.2 AQUASCOPE PRODUCTION SYSTEM

The AQUASCOPE products are based on a multi-algorithm processing chain developed for the Copernicus Marine High-Resolution Ocean Colour service. The processing has been adapted to the Terrascope infrastructure and optically complex coastal waters found in the Southern North Sea.

Spatial Coverage:

The service covers the Belgian North Sea coastal waters including inland estuaries and ports within the region (49°N-53°N, 2°W-5°E; Figure 1).

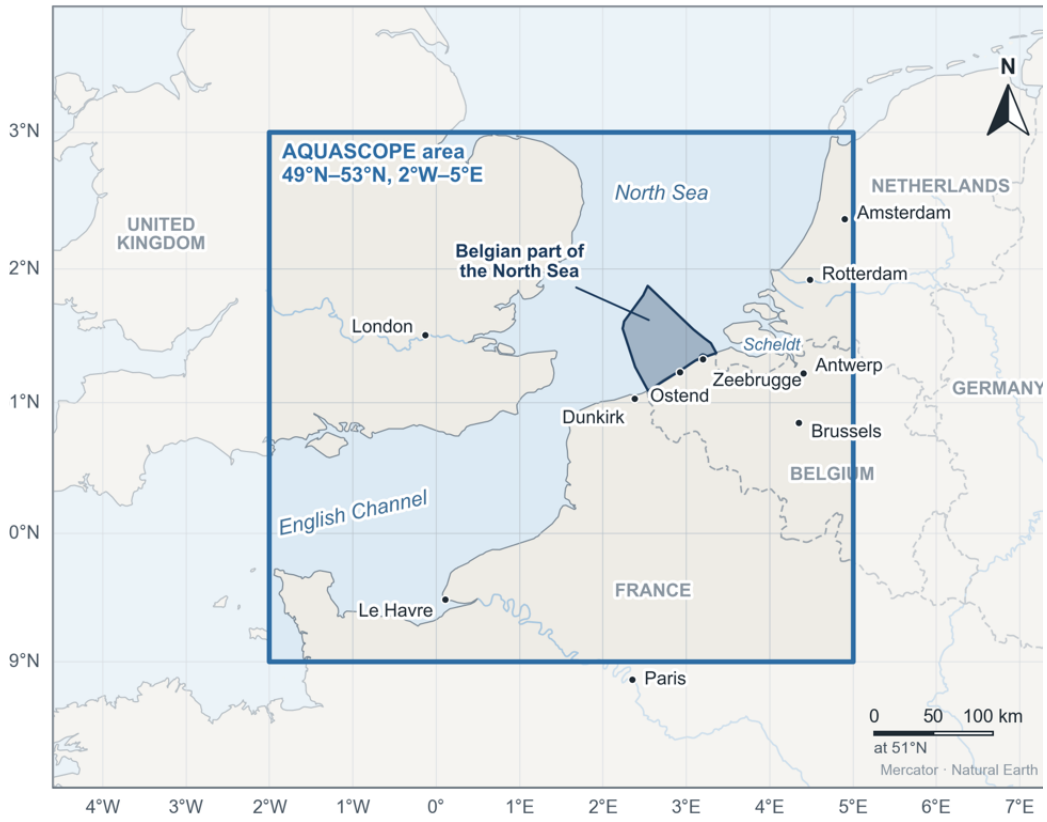


Figure 1: Region covered by the AQUASCOPE service.

Spatial Resolution:

Data are provided at multiple spatial resolutions:

- 10m resolution for Sentinel-2/MSI products (RRS, SPM, TUR)
- 30m resolution for Landsat-8/9 products (RRS, SPM, TUR, SST)
- 60m resolution for the Sentinel-2/MSI CHL product
- 100m resolution for multi-sensor fusion products using both Sentinel-2/MSI and Sentinel-3/OLCI (SPM, TUR, CHL)
- 300m resolution for Sentinel-3/OLCI products (RRS, SPM, TUR, CHL)
- 1000m resolution for Sentinel-3/SLSTR (SST)

Temporal Coverage:

- Archive: 2015 to present
- Near Real-Time (NRT): <24-hour latency
- Products: Daily (L3D, L4D), Monthly (L4M), Yearly (L4Y), Long-term climatology with anomalies

2.3 INPUT PRODUCTS

The AQUASCOPE service processes Level-1 and Level-2 satellite data from multiple sensors into L3/L4 products:

Sentinel-2A/B MSI:

- Input: Level-1C Top-of-Atmosphere reflectance
- Bands: All 13 bands for the pixel classification and the atmospheric correction; the RRS products contain the bands at 443, 490, 560, 665, 704, 740, 783 and 865 nm; SWIR bands B10 (1375 nm) and B11 (1610 nm) for the top-of-atmosphere glint correction and the quality flags
- Spatial resolution: 10m (bands 2,3,4,8), 20m (bands 5,6,7,8A,11,12), 60m (bands 1,9,10)
- Revisit: 2–3 days or less over the Belgian coast (Sentinel-2A, 2B and 2C)

Sentinel-3A/B OLCI:

- Input: Level-1B Full Resolution (EFR) Top-of-Atmosphere radiance
- Bands: All 21 OLCI bands
- Spatial resolution: 300m
- Revisit: daily (with A&B constellation)

Sentinel-3A/B SLSTR:

- Input: Level-2 WST (sea surface temperature, GHRSST L2P format)
- Bands: SST retrieved by EUMETSAT in the WST product from the thermal infrared bands S7 (3.7 µm), S8 (10.8 µm) and S9 (12 µm)
- Spatial resolution: 1000m (SST grid)
- Revisit: daily (with A&B constellation)

Landsat-8/9:

- Input: Level-1 (Collection 2) Top-of-Atmosphere reflectance; Level-2 Surface Temperature (Collection 2, L2SP) for SST
- Bands: OLI visible, NIR and SWIR bands; TIRS Band 10 only through the Level-2 Surface Temperature product
- Spatial resolution: 30m (optical), 30m (thermal)
- Revisit: 8 days (16 days per satellite)

3 PROCESSING STEPS

Figure 2 shows the processing steps from Level-1 to the L3D and L4 water products; each step is described in the following sections.

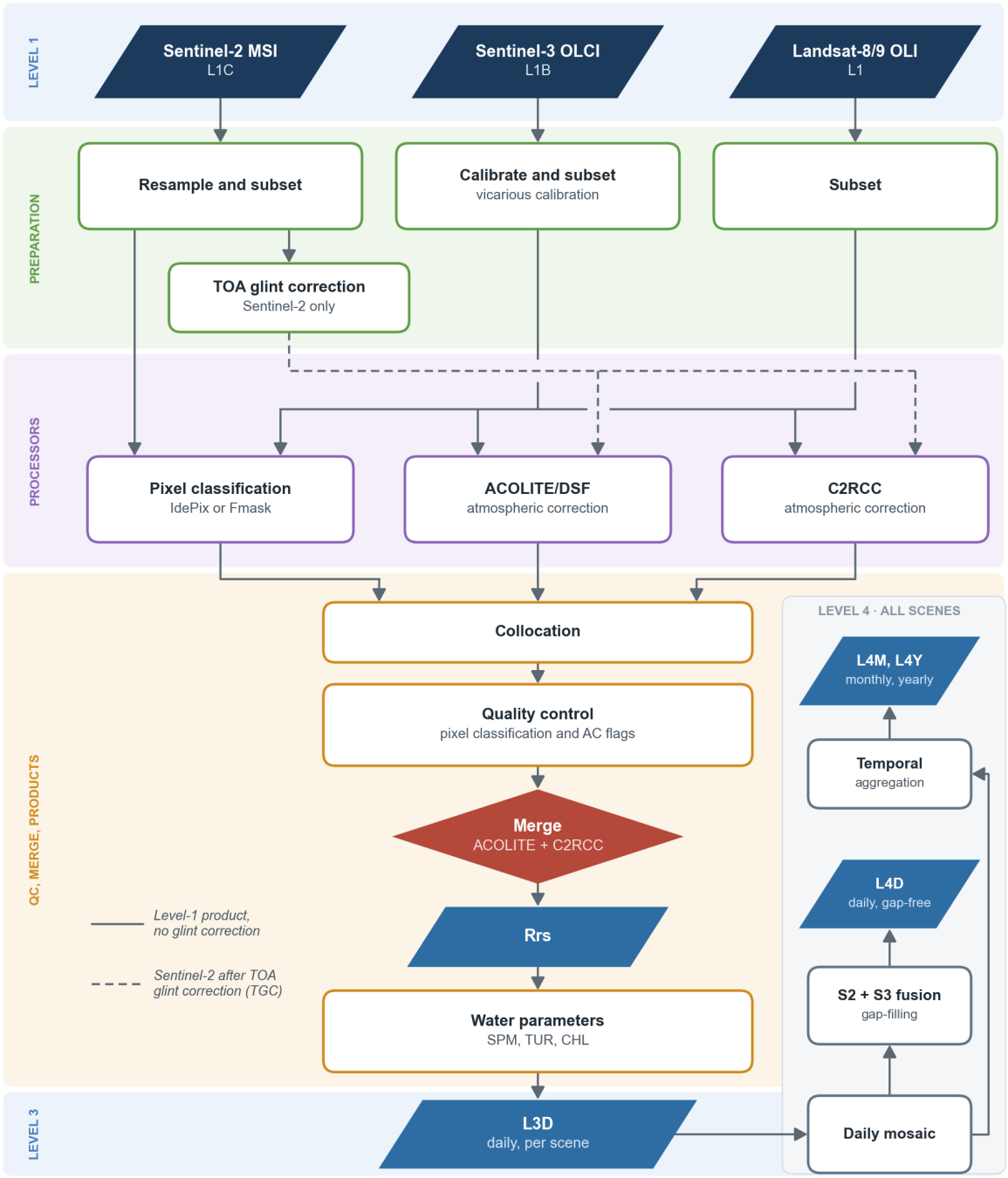


Figure 2: Processing steps from Level-1 to the L3D and L4 water products for Sentinel-2/MSI, Sentinel-3/OLCI and Landsat-8/9/OLI. Solid lines: Level-1 products without glint correction; dashed lines: the Sentinel-2 product after the top-of-atmosphere glint correction (TGC, Sentinel-2 only), the input of ACOLITE and C2RCC. The Sentinel-2 pixel classification (IdePix) uses the product without TGC, as IdePix was trained on data without glint correction.

3.1 PIXEL CLASSIFICATION

The first processing step identifies valid water pixels and flags problematic observations. The AQUASCOPE service uses IdePix version 9.0.6. IdePix provides cloud masking and cloud shadow identification. However, there are other situations which are identified such as floating vegetation, snow and ice, and the land-water distinction also needs to be performed taking temporary water bodies (e.g. intertidal areas, lagoons) into account. These masks are generated based on L1 data, and they are critical for the automated processing of Level 3 and 4 products, when such masks need to be applied to prevent large errors in spatio-temporal averages. The IdePix processors for Sentinel-2/MSI (Wevers et al., 2021), Sentinel-3/OLCI and Landsat-8/9/OLI (version 9.0.6), available as SNAP processors, are used here; for Landsat, Fmask 5.0.1 can be used instead. The classification is complemented by quality tests coming from the Atmospheric correction (AC) algorithms and additional tests in the L3 to L4 processing step. IdePix uses several spectral tests for the identification of cloud, haze, floating vegetation or land-influenced pixels. For Sentinel-2, the IdePix cloud shadow identification depends primarily on a correct cloud mask for which the areas of potential cloud shadow based on the illumination geometry are identified. A clustering of these areas provides the darkest pixels which are flagged as cloud shadow which is then combined with shifting cloud pixels along the illumination path until the minimum of the mean value in reflectances is reached. The results of both methods are combined in a final cloud shadow flag.

Classification categories:

- **Cloud:** Spectral tests on brightness and whiteness identify sure and ambiguous clouds; a buffer is added around them
- **Cloud shadow:** Geometric algorithm projects cloud shadows based on illumination geometry and identifies darkest pixels in potential shadow areas
- **Land:** Land-water distinction with special handling for intertidal zones
- **Cirrus (Sentinel-2):** High reflectance in band 10 (1375 nm), sure and ambiguous
- **Snow and ice:** Bright and white surfaces identified as snow or ice
- **Floating vegetation:** Pixels at risk of floating vegetation (VEG_RISK)
- **Mountain shadow:** Shadows of the terrain

Classes applied. The processor removes the following IdePix classes from the ACOLITE and the C2RCC reflectances: INVALID, LAND, VEG_RISK, CLOUD (which includes the sure and the ambiguous clouds), CLOUD_BUFFER, CLOUD_SHADOW, SNOW_ICE, CIRRUS_SURE, CIRRUS_AMBIGUOUS and MOUNTAIN_SHADOW. Pixels with a sun zenith angle of 75° or more are removed as well.for Sentinel-2 the glint is removed from the top-of-atmosphere reflectance before the atmospheric correction (section Top-of-atmosphere glint correction).

3.2 ATMOSPHERIC CORRECTION

The atmospheric correction processing is a collection of components including:

- Correction for absorbing atmospheric gases;
- Correction for molecular ("Rayleigh") scattering in the atmosphere;
- Correction for aerosol (and multiple aerosol-Rayleigh) scattering in the atmosphere, including potentially absorbing aerosols and taking account of the fact that water reflectance in the near infrared is not negligible ("turbid water effects");
- Correction for reflectance of direct reflection of sky (skyglint, Rayleigh and aerosol) at the air-water interface, often included in the "aerosol" and "Rayleigh" scattering corrections;
- Correction for reflectance of direct sunglint at the air-water interface (still topic of evolution);
- Correction for adjacency effects caused by atmospheric forward scattering of photons from nearby land surfaces (still topic of evolution).

Atmospheric Correction (AC) algorithms, such as C2RCC (Brockmann et al. 2016, Doerffer and Schiller, 2007), ACOLITE/DSF (Vanhellemont, 2019), iCOR (De Keukelaere et al. 2018) and POLYMER (Steinmetz et al., 2011, 2017), were all developed originally to focus on a special case (such as turbid waters and inland waters, Case 2 waters, land surfaces, and sun-glinted Case 1 waters respectively) but have all evolved and become generalized to cover coastal waters. The question of which approach(es) to choose is important and not obvious, and since all atmospheric correction methods are constantly improved and further developed, the best choice may change over time. However, the ACIX-Aqua intercomparison (Pahlevan et al., 2021) for water ACs demonstrated that there is no obvious best method for all tested water bodies. The considered ACs can be subdivided in two groups depending on the approach applied:

- ACs like ACOLITE/DSF (and iCOR) (Vanhellemont, 2019) make no assumption about the water reflectance enabling the return of unusual water reflectance spectra corresponding to optical properties that would not be found in a typical water reflectance model or might lead to an ill-defined mathematical problem with multiple solutions for the more usual water conditions. However, the disadvantage of this approach is that some atmospheric conditions (e.g. severely sunglinted pixels) may be just too challenging.
- ACs like C2RCC (Brockmann et al. 2016, Doerffer and Schiller, 2007) (and POLYMER (Steinmetz et al., 2011, 2017)) have an underlying water reflectance model that assumes that water reflectance will fit some known form (albeit with a certain number of degrees of freedom). The main advantage of the latter approaches is that the additional information provided by a constraint on water reflectance enables a solution to be more easily obtained even in very challenging situations such as high sunglint. These approaches (unless they fail completely) will always produce an R_{RS} spectrum that looks like water. The L2R results can even be relatively insensitive to sensor calibration errors.

Using a single AC would be considered the most straightforward approach. However, to provide maximum ability to achieve high-quality R_{RS} spectra for a maximum number of pixels and yet retain the ability to deal with both unusual water conditions and very challenging atmospheric conditions, the two algorithms, C2RCC (version 9.0.3, normal NN) and ACOLITE/DSF (20260909.0), are used as the baseline L1toL2R approach. These two methods are highly complementary because ACOLITE/DSF makes no assumption about the water reflectance and can therefore achieve good results even for unexpected water types (e.g. dredging plumes, unusual algae species, etc.); whereas C2RCC constrains the water reflectance to correspond to the training data, always giving an R_{RS} spectrum that looks like water. This extra information/constraint on water reflectance, embedded within the C2RCC approach, provides greater retrieval power in the most difficult circumstances (sunglint, highly absorbing waters) but at the expense of imposing a solution for R_{RS} that may not correspond to reality.

TOP-OF-ATMOSPHERE GLINT CORRECTION (SENTINEL-2)

Sun glint and sky glint, the reflection of direct sunlight and skylight at the sea surface, add a signal to the top-of-atmosphere (TOA) reflectance over water that carries no information on the water itself. For Sentinel-2/MSI this signal also produces the typical banding over water: the twelve detectors of MSI view the surface under slightly different angles and, within a detector, the bands do too (because their strips are physically separated on the focal plane). Where the sensor looks towards the sun (the eastern part of the swath, high sun in spring and summer) and at low wind speed, the glint can differ by up to about 10% of the TOA reflectance between adjacent detectors, and spectrally adjacent bands at opposite ends of a detector (e.g. B1 and B2, B8 and B8A) receive different amounts of glint (Vanhellemont, 2021). An atmospheric correction that uses the band-average view geometry leaves these steps in the water reflectance.

AQUASCOPE therefore removes the glint from the TOA reflectance before the atmospheric correction (top-of-atmosphere glint correction, TGC), with the view geometry of each band and detector. The L1C tile is resampled to 10 m while keeping the per-band view zenith and azimuth angles. For each pixel and band, the air–water interface reflectance at TOA is interpolated from the ACOLITE look-up tables (ACOLITE-LUT-202110-MOD2, maritime aerosol model, standard pressure) for the sun geometry, the band-specific view geometry, the wind speed (ECMWF) and the aerosol optical depth at 550 nm (CAMS) of the auxiliary data of the L1C product (both with a minimum of 0.1). The SWIR band B11 (1610 nm), where the water-leaving signal is negligible, serves as reference: where the modelled interface reflectance in B11 exceeds the observed $\rho_t(1610)$, the modelled glint of all bands of that pixel is scaled down by the same factor, so that the correction never removes more than the observed B11 signal. The modelled glint is then subtracted from every band; corrected values are limited to a minimum of 10^{-4}, and pixels with

a sun zenith angle above 80° are set to no data. Both ACOLITE and C2RCC process this glint-corrected product (L1R-TGC).

Figure 3 shows the effect on a Sentinel-2A scene of 19 May 2025 (sun zenith angle 33°). The correction removes the detector banding and most of the wave texture over the open sea. At 665 nm it removes a TOA reflectance of 0.021 over water (median; 0.015–0.028 for 90% of the water pixels), increasing towards the east of the swath, i.e. towards the sun.

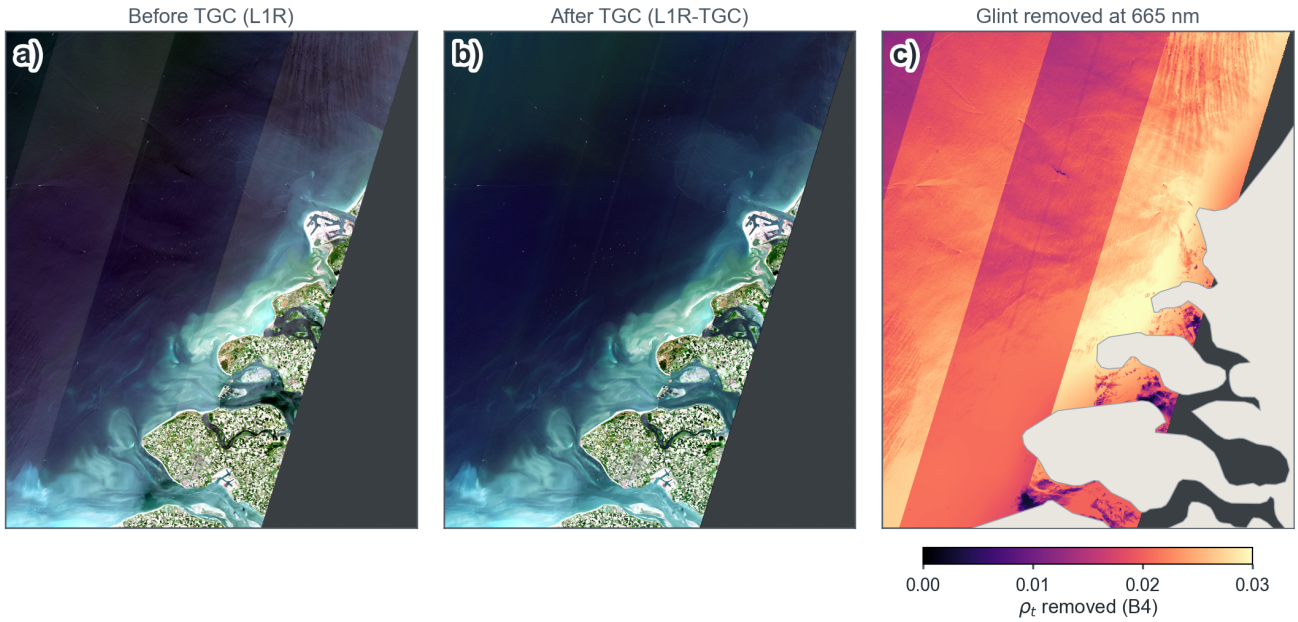


Figure 3: Top-of-atmosphere glint correction (TGC) of Sentinel-2A on 19 May 2025 (tile T31UET, Scheldt mouth): true colour before (a) and after (b) the correction, each with its own colour stretch (b brightened for display), and (c) the glint removed at 665 nm (ρt, band B4), which shows the detector pattern and the increase towards the sun.

QUALITY CONTROL OF THE ACOLITE AND C2RCC REFLECTANCES

Before merging, pixels are removed from the reflectance bands of each atmospheric correction by the IdePix flags and the sun zenith limit of the pixel classification (75°), and by the quality flags of the correction itself:

- **C2RCC:** the flags Rtosa_OOR (top-of-atmosphere spectrum outside the training range of the atmospheric correction network) and Rhow_OOR (water reflectance outside the training range of the IOP network).
- **ACOLITE:** the l2_flags tests of Table 2, computed by ACOLITE on the top-of-atmosphere reflectance ρ_t, and in addition every spectrum with $R_{rs}(865) < -0.001$ sr^{-1}. The non-water, cirrus, high-TOA and out-of-scene tests remove the pixel from both corrections (ACOLITE and C2RCC); the negative-reflectance test and the Rrs(865) limit remove it from ACOLITE only.

Table 2: ACOLITE l2_flags tests applied before merging (ρ_t: top-of-atmosphere reflectance)

Flag value	Test	Sentinel-3/OLCI	Sentinel-2/MSI
1	Non-water (SWIR)	ρ_t(1016 nm) > 0.05	ρ_t(1610 nm) > 0.0215
2	Cirrus	ρ_t(939 nm) > 0.015	ρ_t(1375 nm) > 0.005
4	High TOA reflectance	max ρ_t(440–1050 nm) > 0.3	max ρ_t(400–2500 nm) > 0.3
8	Negative water reflectance	any R_{rs}(440–780 nm) < 0	any R_{rs}(440–710 nm) < 0
16	Out of scene	outside the image data	outside the image data

MERGING OF ACOLITE AND C2RCC

The merged reflectance is a weighted mean of the two corrections (Van der Zande et al., 2023), computed band by band with one ACOLITE weight w per pixel (w = 1: ACOLITE, w = 0: C2RCC):

$$R_{\mathrm{rs,merged}} = w \cdot R_{\mathrm{rs,ACOLITE}} + (1 - w) \cdot R_{\mathrm{rs,C2RCC}}$$

ACOLITE/DSF makes no assumption on water reflectance and handles turbid waters, but in clear waters it struggles due to low measureable signals from the water. C2RCC is constrained to its training data and saturates in very turbid waters. The weight therefore follows two indicators, both taken from C2RCC, because indicators from ACOLITE follow its patchy aerosol residuals:

- **Turbidity**, the C2RCC R_{rs}(865): the weight w_{turb} rises from 0 at $R_{rs}(865) \leq 3\times10^{-4}$ sr^{-1} (clear waters) to 1 at $R_{rs}(865) \geq 1.5\times10^{-3}$ sr^{-1} (turbid waters), the range where ACOLITE and C2RCC agree best (within about ±7% at 560 nm for OLCI).
- **Saturation of C2RCC**, the C2RCC ratio $R = R_{rs}(560)/R_{rs}(865)$: in very turbid waters C2RCC saturates in the green while its R_{rs}(865) can stay low. The weight w_{sat} is 1 at a ratio $R \leq 5$ and 0 at $R \geq 10$.

Between its limits each weight changes logarithmically, as in the band switching of Novoa et al. (2017), and the larger of the two is used, each limited to the range 0 to 1:

$$w_{\mathrm{turb}} = \frac{\log\left(\frac{R_{\mathrm{rs}}(865)}{3 \times 10^{-4}}\right)}{\log(5)}$$

$$w_{\mathrm{sat}} = 1 - \frac{\log\left(\frac{R}{5}\right)}{\log(2)}$$

$$w = max(w_{\mathrm{turb}}, w_{\mathrm{sat}})$$

The weight map is then smoothed with a Gaussian filter (σ = 1 pixel) that ignores pixels without data, to remove single-pixel jumps caused by noise in the C2RCC near-infrared band. Pixels with w = 1 or w = 0 take the reflectance of one correction unchanged. Four cases are handled

separately: where the ACOLITE $R_{rs}(865)$ is negative (but above –0.001), only Rrs(865) is taken from C2RCC and the other bands keep the weighted mean; where C2RCC has no value, ACOLITE is used; where ACOLITE has no valid spectrum (flagged), C2RCC is used; and where ACOLITE has no valid spectrum and C2RCC is saturated (R < 5), C2RCC cannot be trusted on its own and the pixel gets no value.

The variable Rrs_walgo records which correction was used in each pixel (Table 3):

Table 3: Codes of the Rrs_walgo variable

Code	Correction used
1	ACOLITE (w = 1)
2	Mixed (0 < w < 1)
3	C2RCC (w = 0)
4	ACOLITE, with Rrs(865) from C2RCC (ACOLITE Rrs(865) negative)
5	ACOLITE (no C2RCC value)
6	C2RCC: no valid ACOLITE spectrum
7	No value: no valid ACOLITE spectrum and C2RCC saturated (R < 5)
255	No data (land, flagged or outside the scene)

The thresholds were set on Sentinel-3/OLCI scenes and checked on 13 Sentinel-2/MSI scenes. The same values are used for all sensors, so that Sentinel-2 and Sentinel-3 switch in the same waters on the same day. Figure 4 shows the merge on a Sentinel-2 scene.

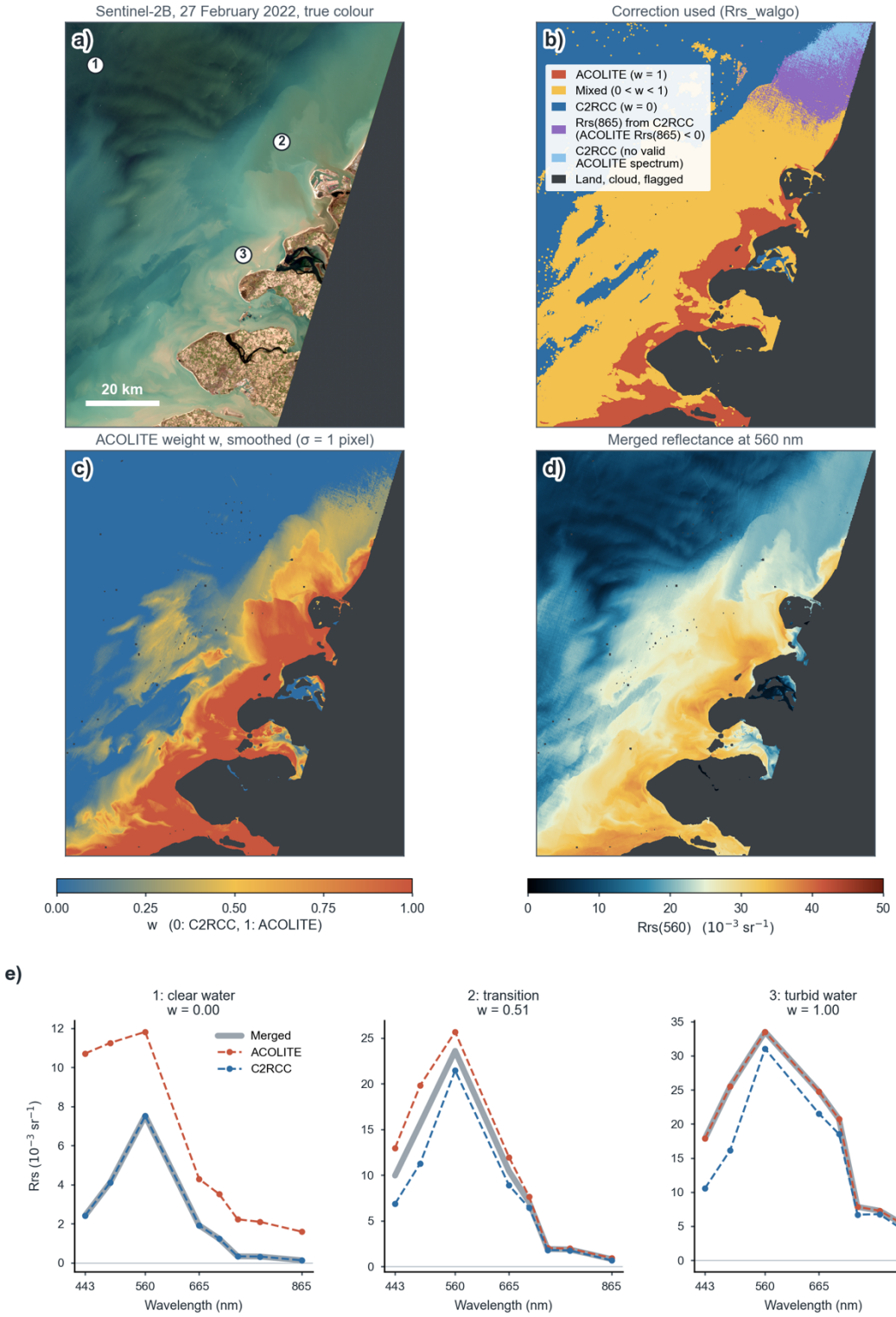


Figure 4: Merging of the ACOLITE/DSF and C2RCC reflectances, Sentinel-2B on 27 February 2022 (Scheldt mouth, 60 m). a) True colour (top-of-atmosphere) with the three example pixels. b) Correction used per pixel (Rrs_walgo). c) ACOLITE weight w after smoothing. d) Merged Rrs(560). e) ACOLITE, C2RCC and merged spectra at the example pixels: 1 clear water (C2RCC), 2 transition (weighted mean), 3 turbid water (ACOLITE).

3.3 SUSPENDED PARTICULATE MATTER (SPM) AND TURBIDITY (TUR)

Nechad et al. (2009, 2010) provided the theoretical basis and functional form (Eq. 1) for SPM and TUR as a function of the water-leaving reflectance ($\rho_w = \pi$ RRS) at a single band, and provided calibration coefficients for all wavelengths λ between 520 nm and 885 nm so that the same basic algorithm can easily be applied to any sensor with a single red or NIR band. The SPM product is generated with the algorithm of Nechad et al. (2010) and the TUR product with the algorithm of Nechad et al. (2009), both applied to the merged ACOLITE/C2RCC RRS (Eq. 1).

$$SPM\ or\ TUR = \left(\frac{A^{\rho} \times \rho_w}{1 - \left(\frac{\rho_w}{C^{\rho}}\right)} \right) + B^{\rho}$$

Eq. 1

Where A^{ρ} (g m^{-3}), B^{ρ} (g m^{-3}) and C^{ρ} (unitless) are constant values at a fixed wavelength which vary by product: SPM or TUR (Table 4). The water-leaving reflectance ρw is defined as RRS x π. For the satellite data application B^{ρ} is set to zero.

Table 4: Coefficients to apply in SPM, TUR algorithm described in Eq. 1.

Parameter	Band (nm) MSI / OLI, OLCI	$A^{\rho}\ (g\ m^{-3})$	C^{ρ}
SPM	665 / 655 865 / 865	342.10 / 346.32 2932.21 / 2929.49	0.19563 / 0.19905 0.21151 / 0.21135
TUR	665 / 655 865 / 865	366.14 / 378.46 3250.32 / 3431.36	0.19563 / 0.19905 0.21151 / 0.21135

MSI: Sentinel-2; OLI: Landsat-8/9. The OLI coefficients are also used for Sentinel-3/OLCI (bands 665 and 865 nm). A is in g m^{-3} for SPM and in FNU for TUR. Coefficients: 2016 calibration (unpublished) of the Nechad et al. (2009, 2010) algorithms, as tabulated in ACOLITE.

Eq. 1 defines a relationship where R_{rs} increases monotonically with SPM, at first linearly and then tends towards an asymptotic or "saturation" reflectance (Luo et al., 2018). Importantly, the slope of the linear relationship and the SPM concentration at which asymptotic behaviour becomes significant depends on the wavelength. Thus, while a single band can be used for SPM estimation, the optimal band depends on SPM concentration – if R_{rs} is too low (e.g. for longer wavelengths in low SPM waters) then the SPM estimation will be significantly affected by noise or errors in R_{rs} – If R_{rs} is too high (e.g. for shorter wavelengths in high SPM waters) then the saturation phenomenon means that R_{rs} becomes insensitive to changes in SPM. This has led to the development of "switching single band algorithms" (Novoa et al., 2017) using the basic single band formulation of (Nechad, Ruddick, and Park, 2010) but with different wavelengths used at different SPM concentrations and typically a smooth weighting between two adjacent spectral bands to avoid image artefacts. The Novoa et al. (2017) approach is applied to both the SPM and

TUR products, providing a multi-band SPM and TUR product using two bands (red: 665 nm and near-infrared: 865 nm). The switch is driven by $\rho_w(665)$: the 665 nm retrieval is used for $\rho_w(665) \leq 0.08$, the 865 nm retrieval for $\rho_w(665) \geq 0.12$, with the logarithmic weighting of Novoa et al. (2017) in between.

Figure 5 shows the resulting merged SPM and TUR products generated for the Scheldt mouth (Sentinel-2B, 1 February 2025) using the band switching approach with an indicator map showing which spectral band was used for each pixel. The yellow zone highlights the region of the weighted transition between the 665 nm and 865 nm bands.

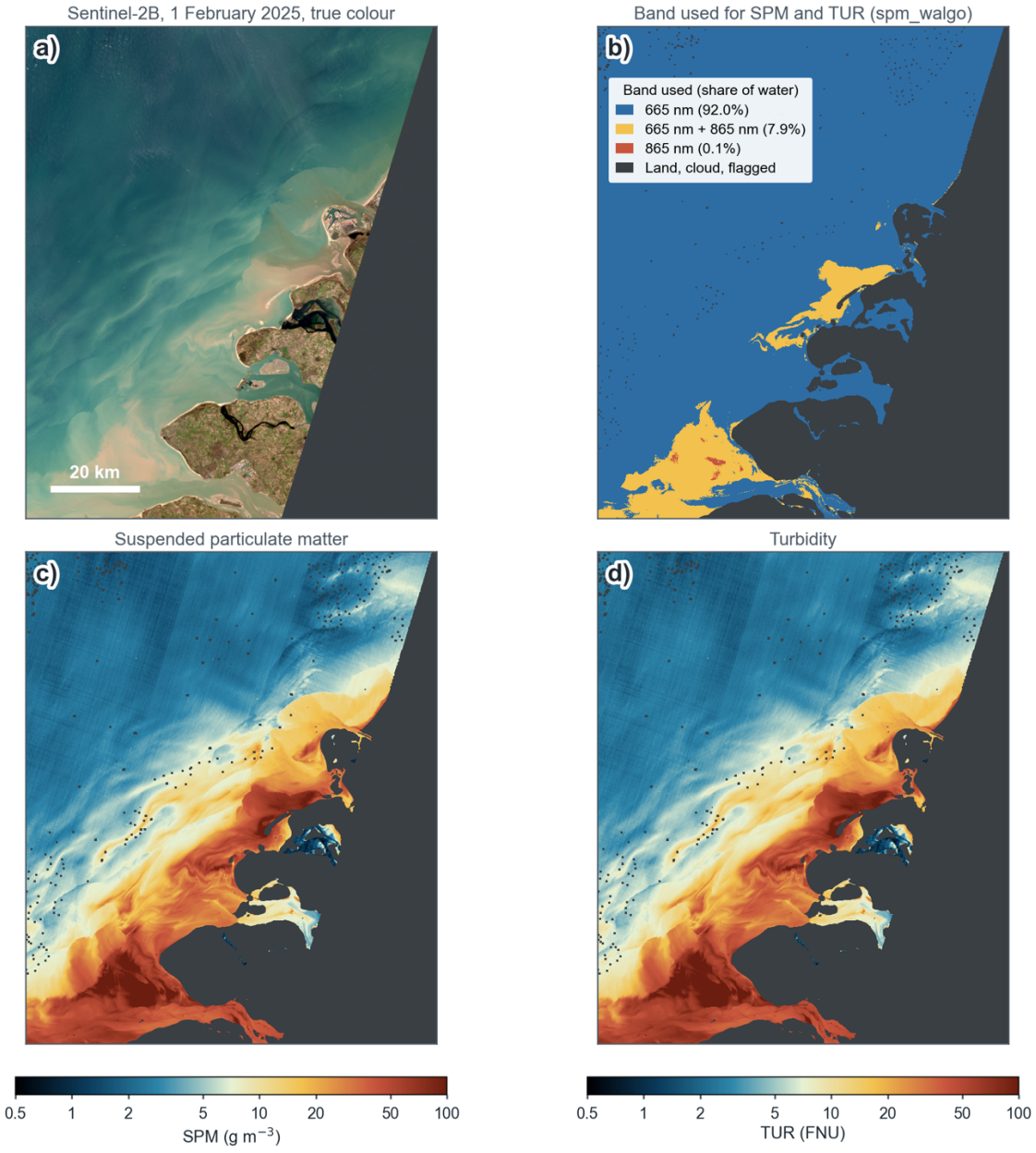


Figure 5: Sentinel-2B scene of the Scheldt mouth on 1 February 2025 (60 m): true colour (a), the spectral band used for each pixel (b) and the resulting SPM (c) and TUR (d) products following the Novoa et al. (2017) approach.

3.4 CHLOROPHYLL-A CONCENTRATION (CHL)

The CHL products of AQUASCOPE are generated for Sentinel-3/OLCI and Sentinel-2/MSI with OCTIS (Ocean Colour Transfer across Imaging Sensors), a machine-learning method developed at RBINS. Retrieving CHL reliably in optically complex coastal waters such as the Belgian coastal zone is challenging: many algorithms exist, each performing well only in some optical conditions. Lavigne et al. (2021) defined a multi-algorithm approach that switches between blue-green band-ratio and NIR-red algorithms according to the water type. This approach is the basis of the Copernicus Marine multi-sensor CHL product for the Atlantic (OCEANCOLOUR_ATL_BGC_L3_MY_009_113, 1 km), which OSPAR uses for the eutrophication assessment of the North Sea in its Quality Status Report 2023. Instead of re-implementing these algorithms for each sensor, OCTIS transfers this trusted product to the sensor: a model learns to reproduce the Copernicus Marine CHL from the sensor's own remote sensing reflectance. The Sentinel-3 and Sentinel-2 CHL are thus on one consistent scale, independent of differences in spectral bands, spatial resolution and atmospheric correction. Figure 6 shows the training of the OCTIS models and their application to the AQUASCOPE products.

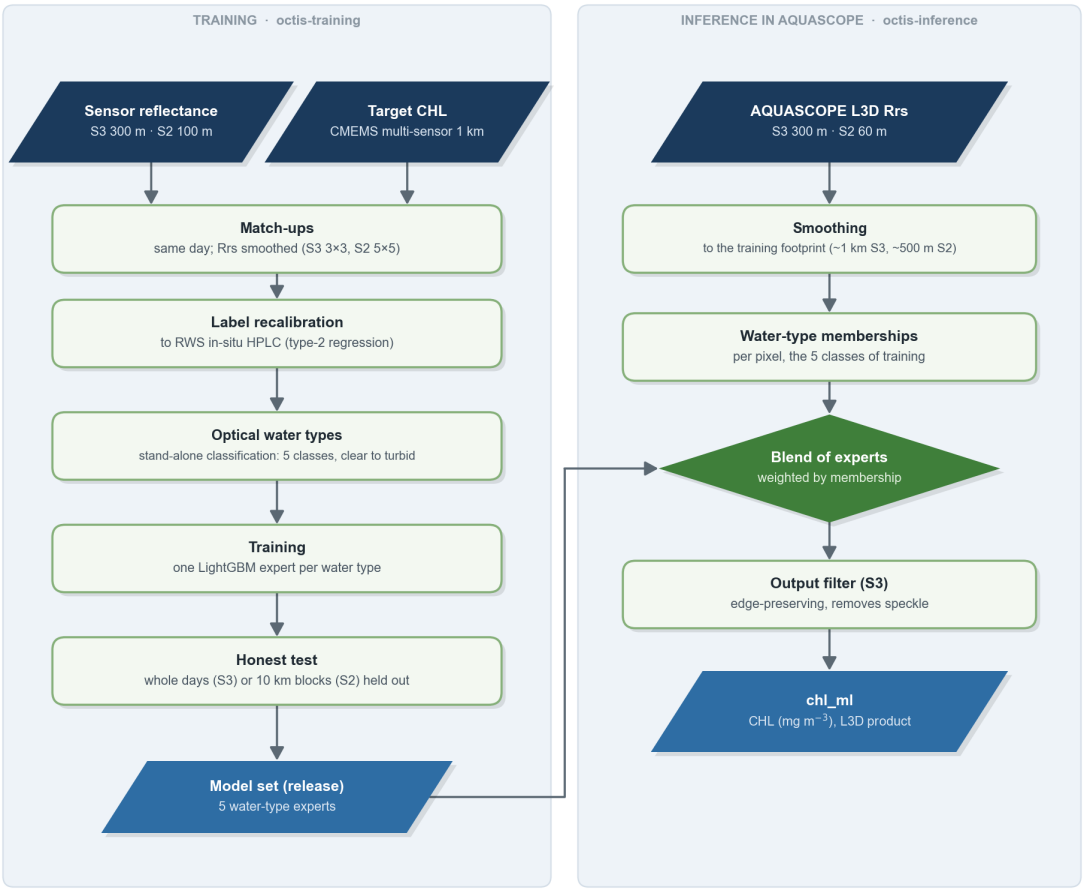


Figure 6: The OCTIS pipeline: training of the water-type experts (left) and their application to the AQUASCOPE L3D products (right).

Training. The training set consists of same-day matchups between the sensor reflectance and the Copernicus Marine CHL. For Sentinel-3, the AQUASCOPE OLCI ACOLITE reflectances at 300 m are used, smoothed with a 3×3 box (about 1 km, the footprint of the target product). For Sentinel-2, ACOLITE reflectances and C2RCC blue and green spectral bands at 60 m are used, smoothed with a 5×5 box (about 500 m). Before training, the Copernicus Marine CHL is recalibrated to *in situ* HPLC measurements of Rijkswaterstaat (RWS, the Netherlands) with a type-2 regression in $\log_{10}$ space, so that the products are on the *in situ* scale.

Each pixel is assigned membership values for five optical water types, from clear to turbid water, with the optical water type (OWT) classification of Chl-CONNECT (Tran et al., 2023). For each water type, a LightGBM model (gradient-boosted decision trees; Ke et al., 2017) is trained to estimate $\log_{10}$(CHL) from the reflectance bands and band ratios (the blue-green maximum band ratio and the green, red-edge and NIR to red ratios; for Sentinel-2 also the C2RCC blue and green bands and their maximum band ratio). Geographic coordinates are deliberately not used as inputs, so that the models remain predictors based on the optics that also hold outside the training area. The training rows are weighted so that rare conditions, such as blooms, are well represented. The models are tested on data never used in training: whole days are held out.

Application to the AQUASCOPE products. For every L3D product the reflectances are first smoothed to the training footprint (Sentinel-3: 3×3 pixels at 300 m; Sentinel-2: products at 60 m are smoothed with a 9×9 box, about 540 m). OWTs are computed and the CHL estimates of the five experts are blended according to these classes. For Sentinel-3, an edge-preserving filter (self-guided filter; He et al., 2013) is applied to $\log_{10}$(CHL); it removes speckle and keeps fronts and bloom peaks. The Sentinel-3 CHL is delivered at 300 m, the Sentinel-2 CHL at 60 m with an effective resolution of about 500 m. The current products use the OCTIS model sets 1.00 (Sentinel-3) and 1.03 (Sentinel-2). Figure 7 shows the OCTIS CHL and the dominant optical water type for a cloud-free Sentinel-3 and Sentinel-2 scene.

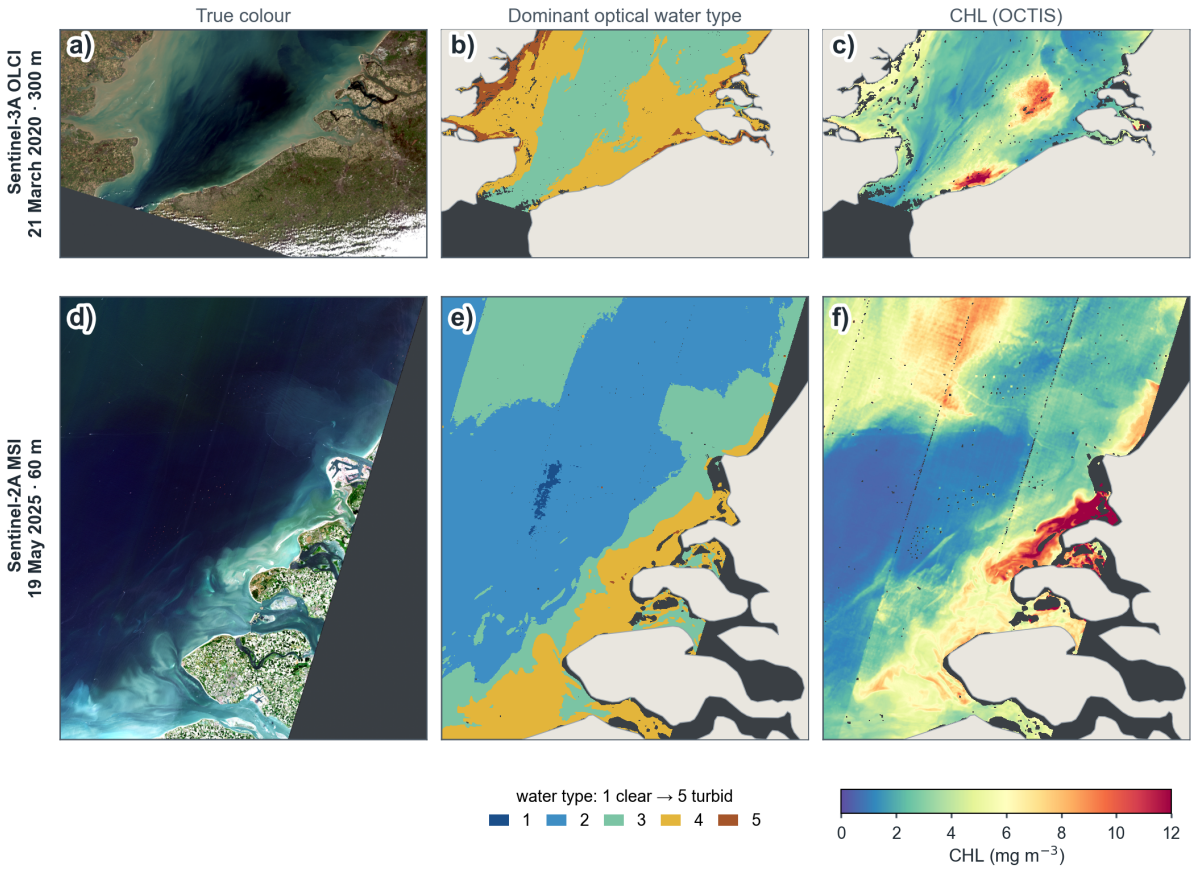


Figure 7: OCTIS CHL on cloud-free days: Sentinel-3A OLCI on 21 March 2020 at 300 m (a–c) and Sentinel-2A MSI on 19 May 2025 at 60 m (d–f): true colour (top of atmosphere; Sentinel-2 after the glint correction), dominant optical water type and CHL. Dark grey: no value (cloud, flagged, outside the image, or no valid ACOLITE spectrum).

3.5 SEA SURFACE TEMPERATURE (SST)

Sea surface temperature (SST) is a fundamental physical parameter for understanding ocean dynamics, coastal processes, and climate variability. High-quality SST observations support applications including marine heat wave detection, thermal fronts mapping, ecosystem monitoring, and validation of oceanographic models. Within AQUASCOPE, we deliver analysis-ready SST products for the Belgian Coastal Zone based on Sentinel-3A/B SLSTR and Landsat-8/9 Level-2 operational SST retrievals. The processing steps are shown in Figure 8.

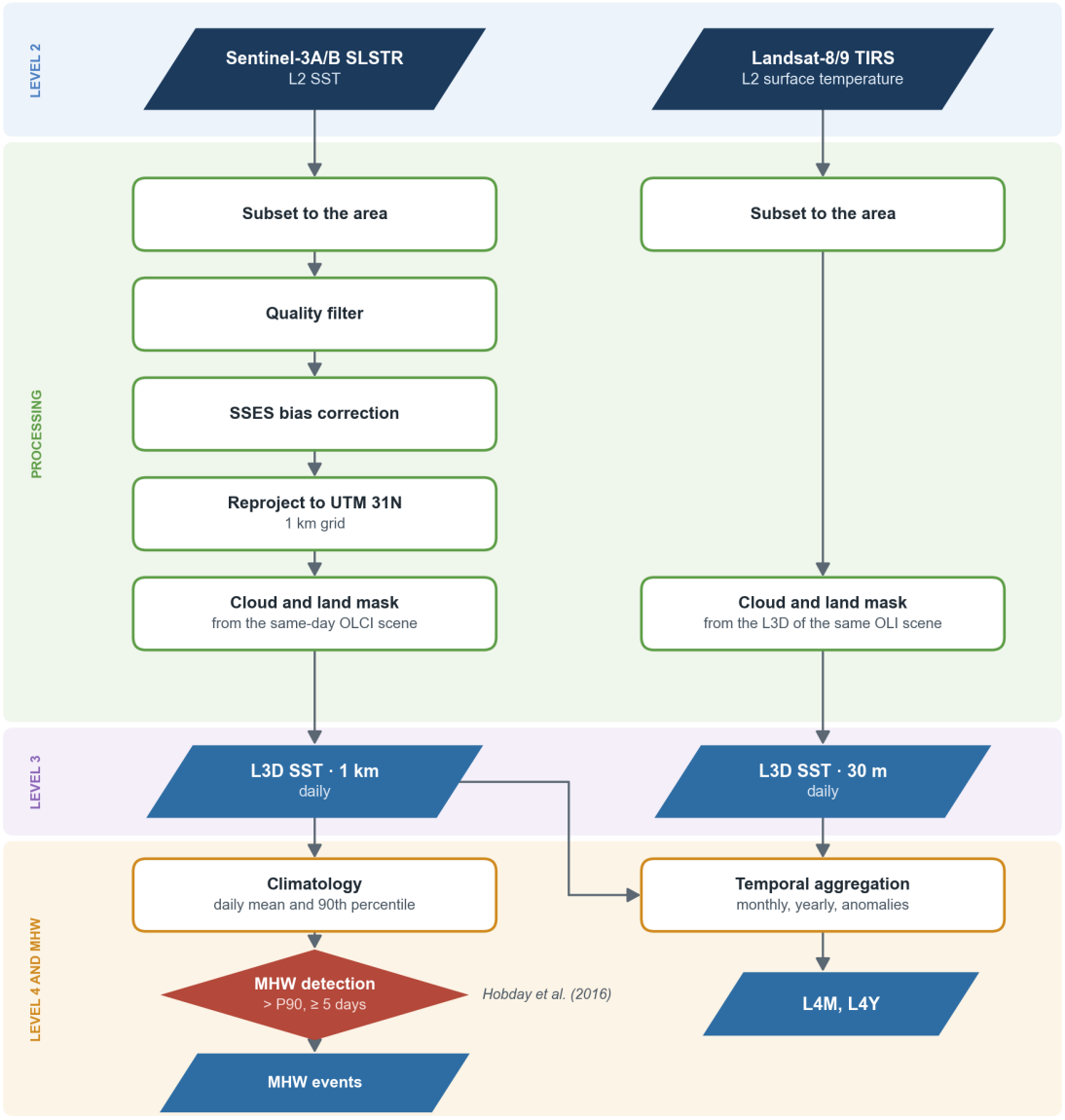


Figure 8: Processing steps for the SST and marine heatwave (MHW) products

Sentinel-3/SLSTR SST:

The SLSTR instrument aboard Sentinel-3 is specifically designed to provide reference-quality SST datasets with zero bias and an uncertainty of ±0.3 K, ensuring consistency with Essential Climate Variable (ECV) requirements. By reprojecting the operational SLSTR L2 SST products to the AQUASCOPE grid and applying robust quality control filtering, we provide spatially consistent, cloud-free SST fields optimized for Belgian coastal waters. AQUASCOPE uses the operational Sentinel-3 SLSTR Level-2 WST (Water Surface Temperature) product generated by EUMETSAT. These products provide pixel-level SST retrievals from thermal infrared brightness temperatures using physically-based regression coefficients derived from radiative transfer modelling.

The SLSTR WST product includes a pixel-level quality level ranging from 0 (no data) to 5 (best quality). AQUASCOPE retains pixels with quality level 4 or 5 and removes pixels flagged as inland water (lake) in the l2p_flags; from processing baseline 004 onwards, the nadir-only retrieval is used. Clouds and land are further masked with the pixel mask (FLAG) of the AQUASCOPE L3D product(s) of the same Sentinel-3 overpass, derived from OLCI and IdePix, regridded by nearest neighbour to the SST grid. Scenes with less than 1% valid pixels in the area are not delivered.

The SLSTR WST product includes sensor-specific error statistics (SSES) providing a bias correction and standard deviation for each SST retrieval. AQUASCOPE applies the SSES bias correction to all retained SST pixels. This correction accounts for residual systematic biases between different algorithm types (N2, N3, D2 and D3; N2 and N3 only for the nadir-only retrieval) and ensures harmonization between Sentinel-3A and Sentinel-3B observations.

The corrected SST is resampled by nearest neighbour (radius of influence 1414 m) to the AQUASCOPE grid (UTM zone 31N, 1000 m) and delivered as a Cloud-Optimised GeoTIFF of sea surface skin temperature in kelvin (scale factor 0.005 K).

Landsat8/9-TIRS SST:

High-resolution sea surface temperature (SST) information is required to resolve fine-scale thermal patterns in coastal waters, including tidal fronts, river plumes, harbor dynamics, and localized thermal discharges. Landsat 8/9 provide thermal infrared observations at 100 m native resolution, which complement the medium-resolution Sentinel□3 SLSTR SST by adding spatial detail in the nearshore zone. AQUASCOPE therefore derives high-resolution SST products from the standard USGS Landsat Collection-2 Level-2 Surface Temperature (ST) product.

AQUASCOPE uses the USGS Landsat Collection-2 Level-2 Surface Temperature (ST) products for Landsat 8 OLI/TIRS and Landsat 9 OLI-2/TIRS-2. These products are Analysis Ready Data (ARD)

compliant and provide atmospherically corrected land surface temperature per pixel in Kelvin, derived from the TIRS thermal band(s) and auxiliary datasets. The USGS Landsat Surface Temperature algorithm uses TIRS Band 10 (single-channel algorithm),, ASTER Global Emissivity Database (GED), ASTER NDVI-based emissivity, and atmospheric profiles to estimate per-pixel surface temperature. Although the algorithm is configured for generic land surface applications, validation studies show that the Collection-2 Level-2 ST product also provides usable water surface temperature in coastal zones, with typical unbiased RMSD of order 1–2 K relative to *in situ* water temperatures, and warm biases around 1–2 K for the standard L2 product.

We convert the standard ST product into an analysis-ready SST product by applying water masks, quality filtering and cropping to the AQUASCOPE area. Clouds (and cloud shadows) and land are masked using the pixel mask (FLAG) of the corresponding AQUASCOPE L3D 30m product(s), derived from OLI and FMask 5.0.1. Scenes with less than 1% valid pixels in the area are not delivered.

The masked SST keeps the 30 m UTM grid of the USGS product (the TIRS data are acquired at 100 m and resampled to 30 m by USGS) and is delivered as a Cloud-Optimised GeoTIFF of surface temperature in kelvin (scale factor 0.005 K).

3.6 RGB IMAGERY

True-colour and false-colour RGB composite images provide intuitive visual representations of satellite observations that support qualitative interpretation, quality control, and communication of ocean colour products to non-specialist users. Within AQUASCOPE, RGB composites are generated from atmospherically corrected Sentinel-2 MSI and Sentinel-3 OLCI surface reflectance products to enable visual inspection of water colour variability, identification of optical features (fronts, plumes, blooms), and validation of automated classification algorithms.

Sentinel-2/Sentinel-3 RGB composites are generated from atmospherically corrected Level-2 remote sensing reflectance using the natural colour bands:

- Red channel: R_{rs}(665 nm)
- Green channel: R_{rs}(560 nm)
- Blue channel: R_{rs}(490 nm)

Standard ocean colour RGB scaling ($R_{rs,max}$ = 0.016, optimized for Case 1 waters) produces oversaturated images in highly turbid Belgian coastal waters where RRS can exceed 0.03 sr^{-1}. AQUASCOPE applies elevated $R_{rs,max}$ thresholds (0.04–0.05) and gamma correction (gamma =

1.2–1.3) to preserve contrast and colour discrimination across the full turbidity gradient from offshore (SPM ~ 5 g m^{-3}) to the zone of maximum turbidity (SPM > 100 g m^{-3}).

4 TEMPORAL COVERAGE

4.1 TEMPORAL AGGREGATION

Daily Products (L3D):

- Multi-sensor fusion within same day
- Overlap handling: Preference to lower solar zenith angle observation
- Quality flag preservation
- All parameters available

Monthly Products (L4M):

- Temporal aggregation of all daily products in calendar month
- Cloud-masked pixel averaging
- Quality flag combination (logical OR of all flags)
- All parameters available
- Delivery: Monthly in NRT mode

Yearly Products (L4Y):

- Temporal aggregation of all daily products in calendar year
- Growing season statistics (April-September) for eutrophication assessment
- All parameters available
- Used for long-term climatology

Anomaly Products:

- Daily anomaly = Daily value - Long-term monthly mean for that day-of-year
- Monthly anomaly = Monthly mean - Long-term monthly mean
- Expressed as absolute difference and percentage difference

5 VALIDATION FRAMEWORK

5.1 RADIOMETRIC *IN SITU* DATA

The radiometric *in situ* dataset consists of water spectra collected the Pan-and-Tilt Hyperspectral Radiometer system (PANTHYR, Vanhellemont, 2020b; Vansteenwegen et al., 2019) for the period 1/10/2019 – 15/7/2020. Two autonomous PANTHYR systems were deployed at the Thornton

Bank on the Cpower transformation station (CPower, 51.5328°N, 2.9551°E) and at Research Tower 1 (RT1) near Oostende (RT1, 51.2464°N, 2.9193°E), and are measuring independently every 20 minutes during daytime. The water at Cpower is fairly clear. The water at RT1 is turbid with tidal variability and with an occasional outflow from the port of Oostende (Belgium) reaching the site. Matchups the PANTHYR stations were extracted from shifted locations near the deployment towers, to avoid platform effects such as direct pixel contamination and shadows, as well as in-water wakes.

***In situ* stations**

- **Oostende RT1** (51.2464°N, 2.9193°E): Turbid tidal waters with port outflow
- **Zeebrugge MOW1** (51.3606°N, 3.1182°E): Coastal waters near major port
- **Thornton CPower** (51.5328°N, 2.9551°E): Offshore wind farm location

Hypernets characteristics:

- Hyperspectral measurements (350-1050 nm, 1.5 nm sampling)
- Automated measurements every 20 minutes
- Pan-and-tilt system avoids platform shadowing
- Quality control following WATERHYPERNET protocols
- Used for RRS validation at Oostende (O1BE) and Thornton Bank (TBBE)

5.2 BIOGEOCHEMICAL *IN SITU* DATA

The biogeochemical products (CHL, SPM) are validated against two *in situ* datasets from the southern North Sea (Table 5).

Table 5: *In situ* data used for the validation of the biogeochemical products.

Source	Parameters	Region	Data access
Belgian monitoring programme, RBINS (campaigns of the research vessel Belgica)	CHL (HPLC), SPM	Belgian part of the North Sea	Belgian Marine Data Centre (BMDC), RBINS: https://www.bmdc.be
Rijkswaterstaat (RWS): MWTL monitoring stations and ship campaigns	CHL (HPLC)	Dutch part of the North Sea	Rijkswaterstaat Waterinfo: https://waterinfo.rws.nl

The Belgian data were collected by RBINS during the monitoring campaigns of the research vessel Belgica and are made available through BMDC; they are the main reference for SPM. For CHL, the validation relies mainly on the RWS dataset: it contains many more samples, all analysed by HPLC, and the Dutch coastal waters are optically very similar to the Belgian coastal waters. The RWS data were also used to recalibrate the training label of the OCTIS CHL models (section 3.4).

6 VALIDATION ANALYSIS

6.1 MATCHUP ANALYSIS AND STATISTICAL MEASURES

Validation analysis refers to the estimate of the statistical parameters listed in Table 6, using *in situ* observations.

Matchup Extraction Protocol:

Adapted from Bailey and Werdell (2006); the protocol of each product is given in its subsection:

- Maximum time window: 3 hours
- Spatial extraction: 3×3 pixel window around the *in situ* position, at the resolution of the product
- Coefficient of Variation (CV) < 0.15 for valid matchup
- Exclude pixels flagged as: cloud, cloud shadow, land, ice, invalid

Table 6: Metrics used to compare the estimated (satellite-based) X_(i,j=1..N)^E dataset to a reference (*in situ*) X_(i,j=1..N)^M dataset. For log-normally distributed variables (i.e. SPM, TUR and CHL) both datasets are log-transformed prior to computing the metrics.

Name	Definition
Estimated dataset mean ($\bar{X}^E$)	$\bar{X}^E = \frac{1}{N}\sum_{i=1}^{N} X_i^E$
Reference dataset mean ($\bar{X}^M$)	$\bar{X}^M = \frac{1}{N}\sum_{i=1}^{N} X_i^M$
Type-2 slope (S)	$S = \frac{\sum_{i=1}^{N}(X_i^E - \bar{X}^E)^2 - \sum_{i=1}^{N}(X_i^M - \bar{X}^M)^2 + \left[\{\sum_{i=1}^{N}(X_i^E - \bar{X}^E)^2 - \sum_{i=1}^{N}(X_i^M - \bar{X}^M)^2\}^2 + 4\{\sum_{i=1}^{N}(X_i^E - \bar{X}^E)(X_i^M - \bar{X}^M)\}^2\right]^{\frac{1}{2}}}{2\sum_{i=1}^{N}(X_i^E - \bar{X}^E)(X_i^M - \bar{X}^M)}$
Type-2 intercept (I)	$I = \bar{X}^E - S \cdot \bar{X}^M$
Determination coefficient (r^2)	$r^2 = \frac{[\sum_{i=1}^{N}(X_i^E - \bar{X}_i^E)(X_i^M - \bar{X}_i^M)]^2}{\sum_{i=1}^{N}(X_i^E - \bar{X}_i^E)^2 \sum_{i=1}^{N}(X_i^M - \bar{X}_i^M)^2}$
Root Mean Square Difference (RMSD)	$RMSD = \sqrt{\frac{\sum_{i=1}^{N}(X_i^E - X_i^M)^2}{N}}$
Centre-pattern Root Mean Square Difference (cRMSD)	$cRMSD = \sqrt{\frac{\sum_{i=1}^{N}\{[X_i^E - \bar{X}^E] - [X_i^M - \bar{X}^M]\}^2}{N}}$
Bias	$bias = \frac{1}{N}\sum_{i=1}^{N}(X_i^E - X_i^M)$
Median Absolute Percentage Difference (MAPD)	$MAPD = median(\left\|\frac{X_i^E - X_i^M}{X_i^M}\right\|)$

Notes:

- Type-2 regression (called also orthogonal regression) minimizes the perpendicular distance between the data and the fitted line, instead of the vertical distance as in Type-1 regression. Type-1 regression assumes that the independent variable (the *in situ* data) is known exactly, when in reality, the *in situ* data are also affected by uncertainties (e.g. problems with *in situ*-data sampling techniques) that are difficult to quantify.
- A slope (S) close to one and an intercept (I) close to zero is an indication that the model compares well with the *in situ* data.
- The Centre-pattern (or unbiased) Root Mean Square Difference describes the error of the estimated values with respect to the measured ones, regardless of the average bias between the two distributions.
- The RMSD is the typical difference between the satellite and the *in situ* values, i.e. the spread of the data points around the 1:1 line; it includes the bias ($RMSD^2 = bias^2 + cRMSD^2$). The RMSD is directly interpretable in terms of measurement units, and so is a better measure of goodness of fit than a correlation coefficient.
- The bias indicator is also directly interpretable in terms of measurement units. The differences are not squared, so negative and positive differences cancel. The bias is not a good indicator of average model performance and might be a misleading indicator of average error. It should be carefully considered taking into account the scatter plot.

6.2 REMOTE SENSING REFLECTANCE (RRS)

The RRS products are validated against the autonomous hyperspectral *in situ* radiometry at Oostende (station O1BE) and Thornton Bank (station TBBE) in the Belgian coastal zone, for 2020–2025. The matchups were extracted with the protocol described above: 197 for Sentinel-3/OLCI (163 scenes, 14 bands), 118 for Sentinel-2/MSI (8 bands) and 42 for Landsat-8/9/OLI (32 scenes, 5 bands). The *in situ* spectra are compared with ACOLITE, C2RCC and the merged AQUASCOPE RRS; the metrics are those of Table 6, computed on R_{rs} in sr^{-1} over all bands together (Table 7, Figure 9) and per band (Figure 10).

Table 7: Validation metrics of the RRS, all bands together (definitions in Table 6; RMSD and bias in sr^{-1}).

Sensor	Correction	Matchups (N)	r^2	Slope	RMSD	Bias	MAPD (%)
Sentinel-3/OLCI	ACOLITE	197 (2758)	0.84	0.92	0.0035	+0.0002	26
Sentinel-3/OLCI	C2RCC	197 (2758)	0.84	0.77	0.0041	-0.0018	27
Sentinel-3/OLCI	**Merged (AQUASCOPE)**	**197 (2758)**	**0.87**	**0.92**	**0.0032**	**-0.0006**	**22**
Sentinel-2/MSI	ACOLITE	118 (944)	0.90	0.94	0.0033	+0.0013	28
Sentinel-2/MSI	C2RCC	118 (944)	0.91	0.85	0.0036	-0.0019	25
Sentinel-2/MSI	**Merged (AQUASCOPE)**	**118 (944)**	**0.92**	**0.98**	**0.0028**	**+0.0001**	**20**
Landsat-8/9/OLI	ACOLITE	42 (210)	0.88	0.88	0.0047	+0.0027	36
Landsat-8/9/OLI	C2RCC	42 (210)	0.92	0.71	0.0057	-0.0040	34
Landsat-8/9/OLI	**Merged (AQUASCOPE)**	**42 (210)**	**0.91**	**0.91**	**0.0033**	**-0.0002**	**18**

For all three sensors the merged RRS agrees best with the *in situ* data: RMSD of 0.0028–0.0033 sr^{-1}, MAPD of 18–22%, a bias close to zero (−0.0006 to +0.0001 sr^{-1}), r^2 of 0.87–0.92 and type-2 slopes of 0.91–0.98. ACOLITE overestimates the RRS (bias +0.0002 to +0.0027 sr^{-1}) and C2RCC underestimates it (bias −0.0018 to −0.0040 sr^{-1}, slopes 0.71–0.85); the merge combines the two and largely cancels these opposite biases.

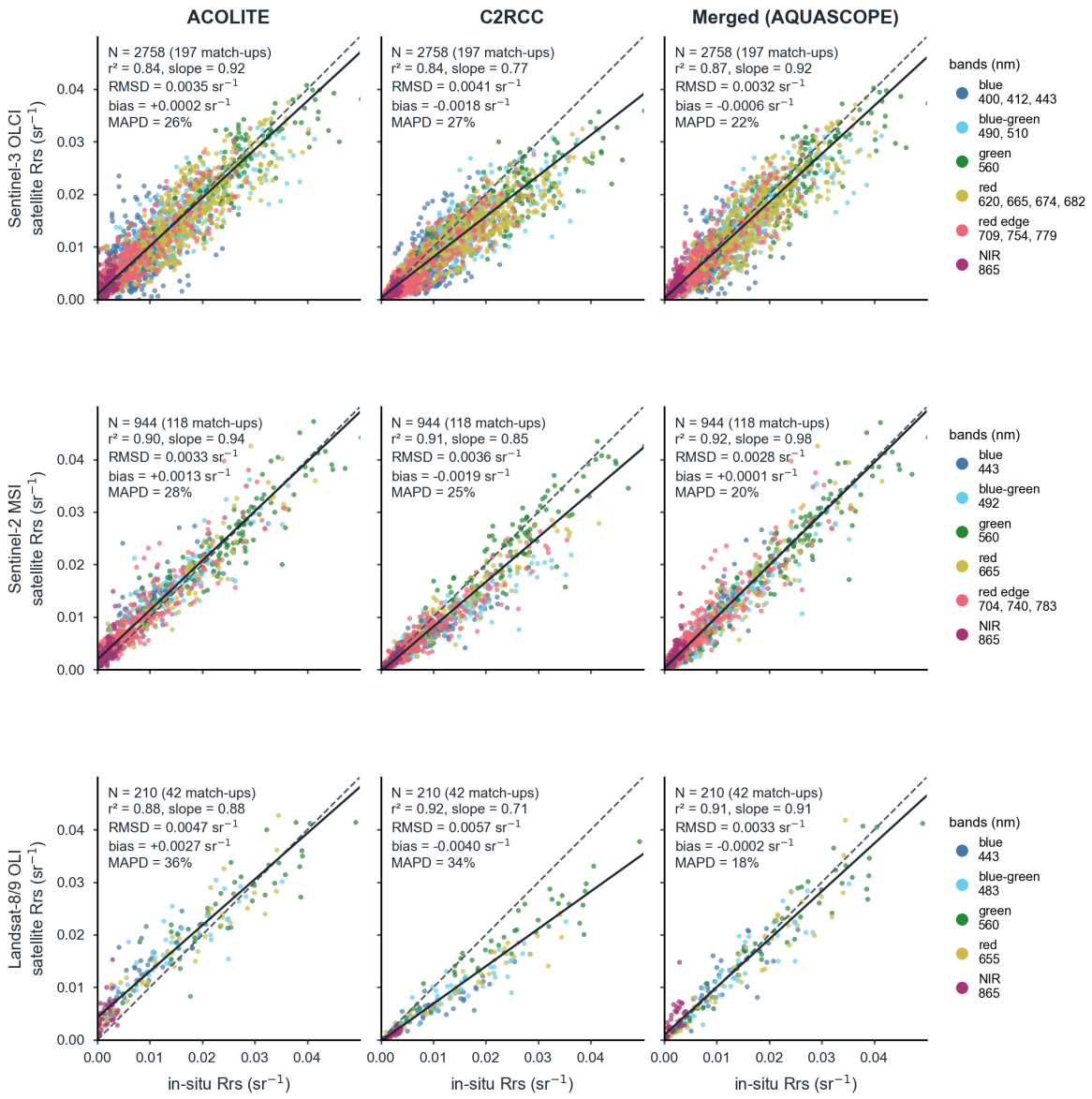


Figure 9: Satellite RRS against *in situ* RRS at Oostende (O1BE) and Thornton Bank (TBBE), 2020–2025, for Sentinel-3/OLCI (top), Sentinel-2/MSI (middle) and Landsat-8/9/OLI (bottom), and for ACOLITE (left), C2RCC (centre) and the merged AQUASCOPE RRS (right). All bands together, coloured by band; dashed line: 1:1; solid line: type-2 regression.

Per band (Figure 10), the merged R_{rs} has the lowest RMSD in nearly all visible bands (MAPD 12–24%); it is slightly low there, most in the green (bias −0.0016 sr^{-1} at 560 nm for OLCI, −0.0015 sr^{-1} for OLI), where the merge weights C2RCC more. In the red-edge and near-infrared bands (740 nm and longer) C2RCC has the smallest differences and the merged R_{rs} is slightly high; the MAPD is larger there (30–42%, 84% at 865 nm for OLI) because the reflectance itself is small, while the absolute differences remain small (RMSD below 0.003 sr^{-1}). The Landsat-8/9 results rest on 42 matchups only.

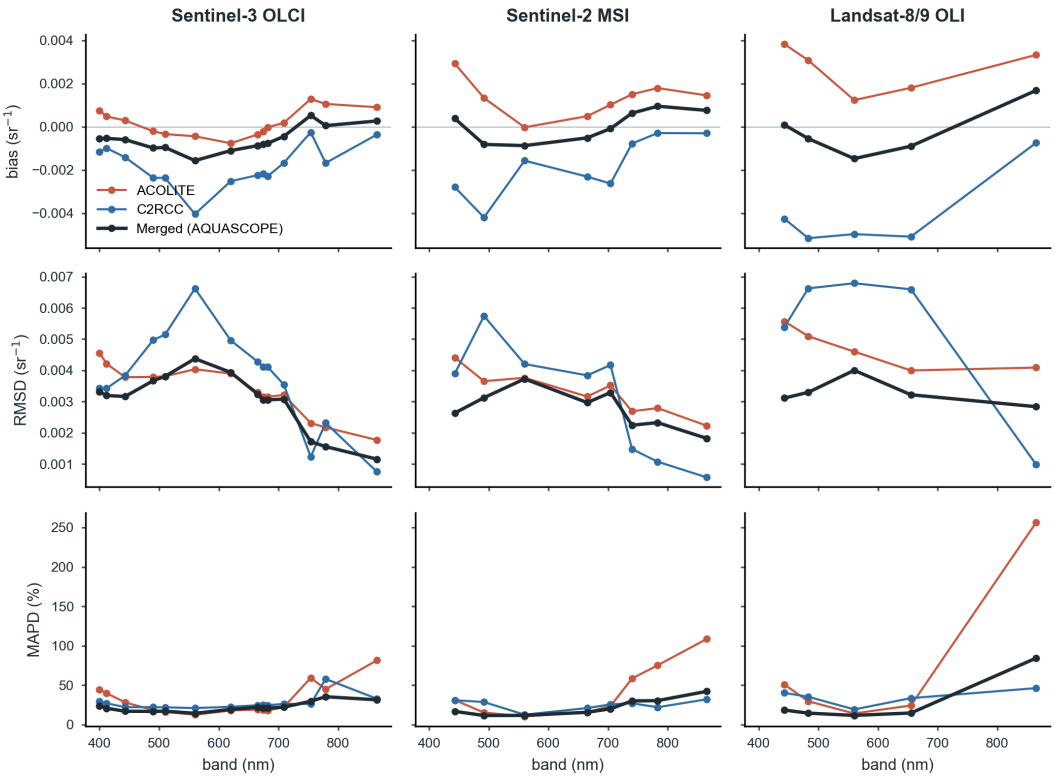


Figure 10: Bias, RMSD and MAPD per band of ACOLITE, C2RCC and the merged AQUASCOPE RRS against the *in situ* RRS, for Sentinel-3/OLCI, Sentinel-2/MSI and Landsat-8/9/OLI.

6.3 CHLOROPHYLL-A CONCENTRATION (CHL)

The CHL products are validated against the RWS *in situ* HPLC data (Table 5 in section 5.2) in the Dutch part of the North Sea, 2019–2025: samples of the Dutch monitoring programme (MWTL) and ad-hoc samples collected as direct matchups for satellite validation (Figure 11). For Sentinel-3/OLCI, a matchup is the 3×3 pixel box around the sample on the same day, with at least 5 valid pixels and a coefficient of variation below 0.15: 255 matchups (196 from the monitoring programme, 59 ad-hoc). For Sentinel-2/MSI, OCTIS is applied to the mean ACOLITE and C2RCC reflectances in the 3×3 pixel box around the RWS sample position, and matchups with flagged or too few valid pixels are removed: 96 matchups (75 from the monitoring programme, 21 ad-hoc; Sentinel-2A, 2B and 2C). The metrics of Table 6 are computed on log10(CHL); the MAPD on CHL itself. The results are given in Table 8.

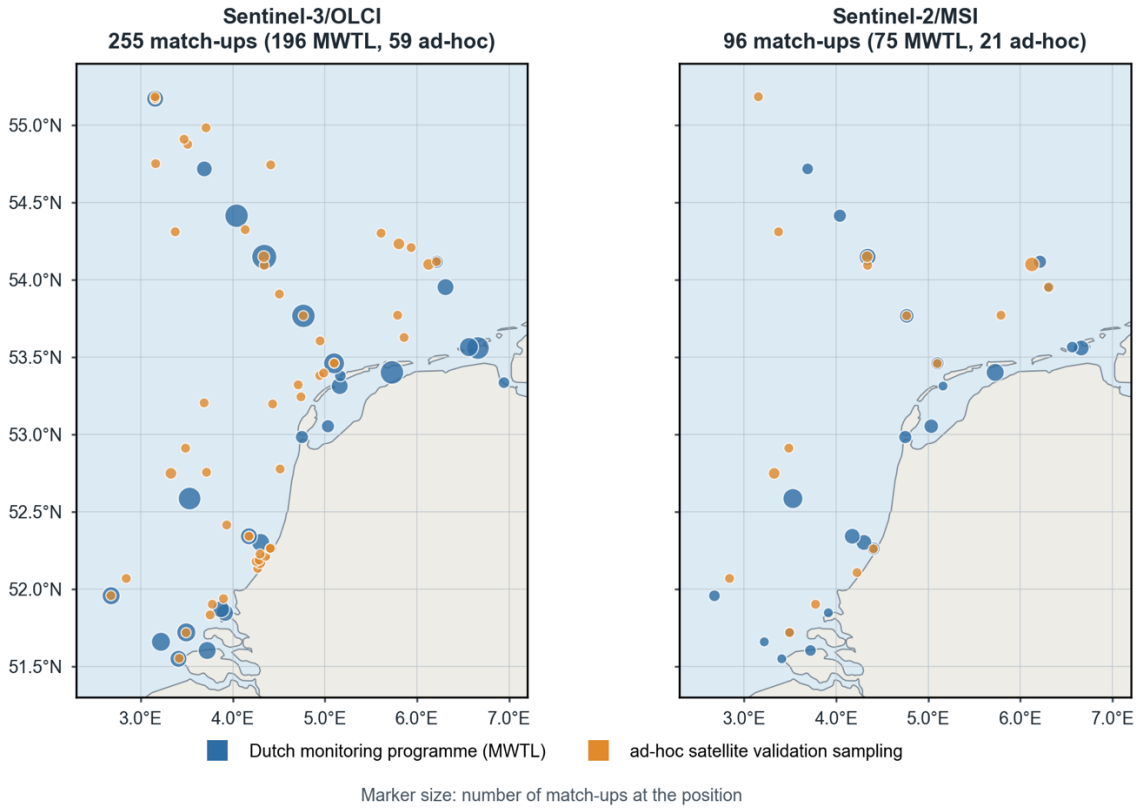


Figure 11: Positions of the RWS CHL matchups for Sentinel-3/OLCI (left) and Sentinel-2/MSI (right); blue: Dutch monitoring programme (MWTL), orange: ad-hoc sampling for satellite validation. Marker size: number of matchups at the position.

Table 8: Validation of the CHL against RWS *in situ* HPLC data: OCTIS and the CMEMS products at the same matchups (metrics of Table 6 on log10(CHL); MAPD on CHL).

Sensor	Product	Matchups	r^2	Slope	RMSD	Bias	MAPD (%)
Sentinel-3/OLCI	**OCTIS (model set 1.00)**	**255**	**0.66**	**0.95**	**0.308**	**+0.021**	**42**
Sentinel-3/OLCI	CMEMS multi-sensor 1 km	255	0.66	0.92	0.338	+0.148	61
Sentinel-2/MSI	**OCTIS (model set 1.03)**	**96**	**0.52**	**0.92**	**0.322**	**+0.048**	**49**
Sentinel-2/MSI	CMEMS HR-OC 100 m	96	0.42	0.94	0.366	+0.074	59

For Sentinel-3, the OCTIS CHL agrees with the *in situ* data over more than two orders of magnitude (0.1 to 50 mg m^{-3}): r^2 = 0.66, type-2 slope 0.95, RMSD 0.31 and bias +0.02 (log10), MAPD 42% (Table 8, Figure 12). The CMEMS multi-sensor 1 km CHL has the same r^2 at these matchups but a larger bias (+0.15) and MAPD (61%); the recalibration of the training label to the *in situ* scale removes this offset. For Sentinel-2, the OCTIS CHL reaches r^2 = 0.52, slope 0.92, RMSD 0.32 and bias +0.05 (log10), MAPD 49%, and agrees better with the *in situ* data than the CMEMS HR-OC CHL at the same matchups (r^2 = 0.42, RMSD 0.37, MAPD 59%).

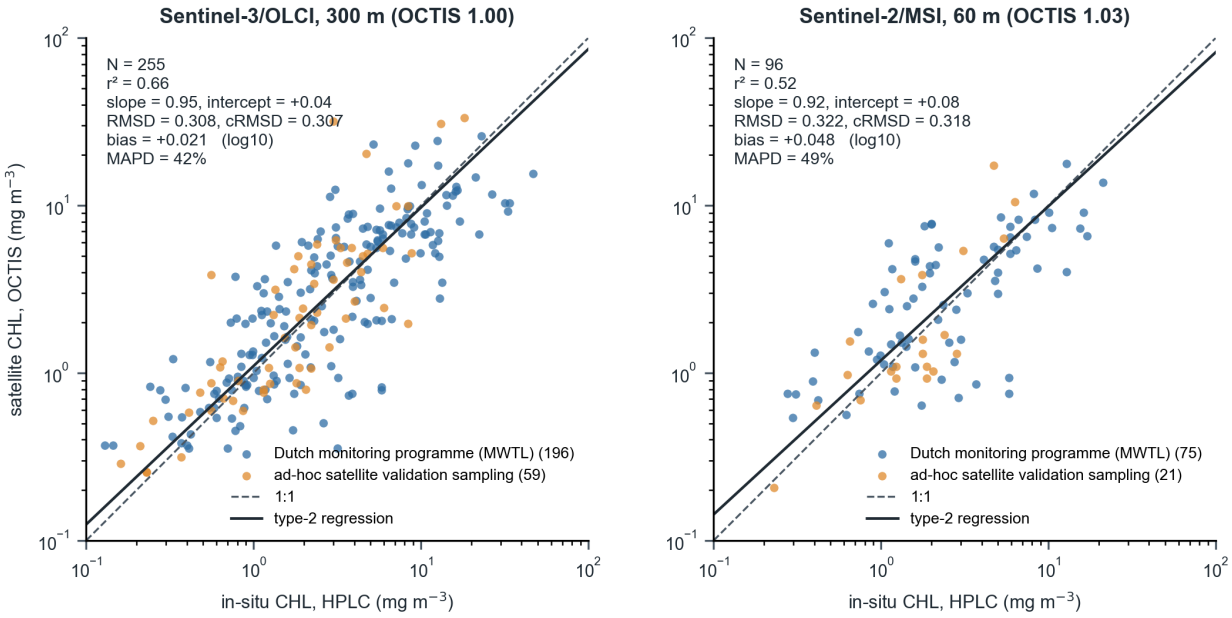


Figure 12: OCTIS CHL against RWS *in situ* HPLC CHL in the Dutch part of the North Sea, 2019–2025: Sentinel-3/OLCI (left, model set 1.00) and Sentinel-2/MSI (right, model set 1.03); blue: Dutch monitoring programme (MWTL), orange: ad-hoc sampling for satellite validation. Dashed line: 1:1; solid line: type-2 regression; metrics on log10(CHL), MAPD on CHL.

Because the training label was recalibrated with RWS data, these data are not fully independent of the OCTIS models. A blocked cross-validation of the recalibration, leaving one station, one year or one dataset out at a time, gives an RMSD of 0.307–0.313 for Sentinel-3, so the results are not driven by this overlap.

6.4 SUSPENDED PARTICULATE MATTER (SPM)

The SPM products are validated against the SPM of the Belgian monitoring programme (RBINS, campaigns of the research vessel Belgica; Table 5 in section 5.2) at three stations from the coast to offshore (Figure 13): MOW1 (51.355°N, 3.131°E, turbid nearshore water off Zeebrugge), W05 (51.411°N, 2.825°E) and W08 (51.460°N, 2.349°E), 2018–2023. A matchup is the satellite SPM in the 3×3 pixel box around the station within 3 hours of the *in situ* sample: 32 matchups for

Sentinel-3/OLCI and 11 for Sentinel-2/MSI. The metrics of Table 6 are computed on $\log_{10}$(SPM), the MAPD on SPM itself. The results are given in Table 9.

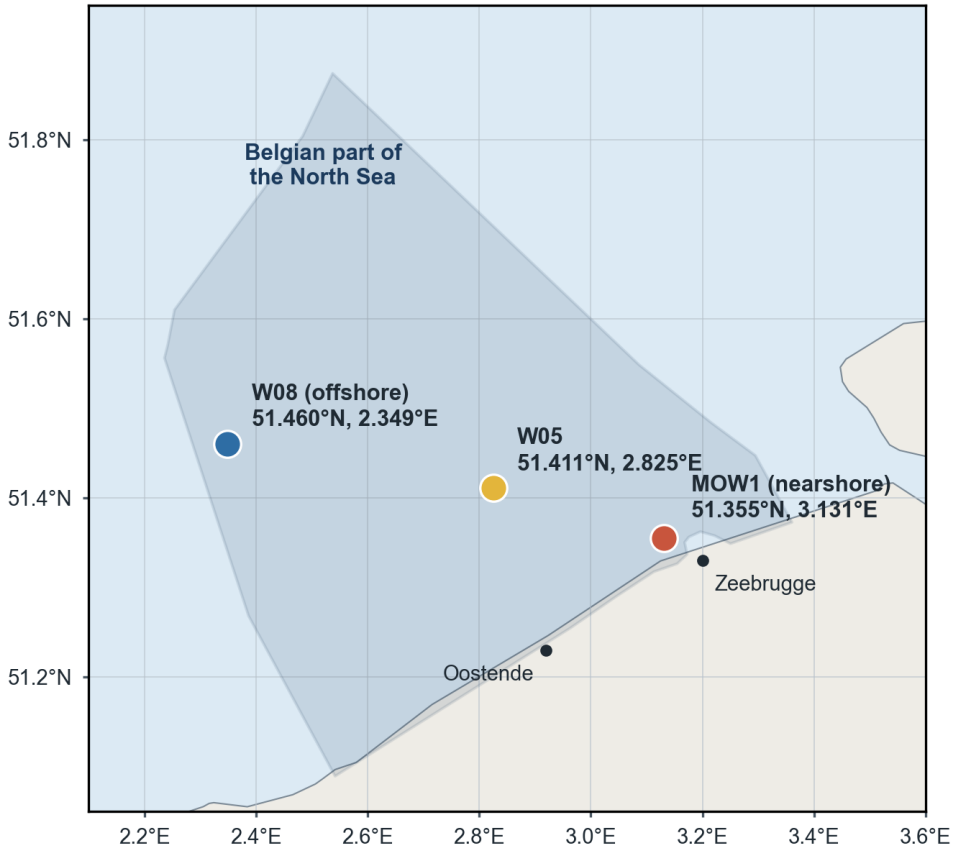


Figure 13: Stations of the Belgian monitoring programme used for the SPM validation: MOW1 (nearshore, off Zeebrugge), W05 and W08 (offshore), in the Belgian part of the North Sea (shaded).

Table 9: Validation of the SPM against the Belgian monitoring programme (metrics of Table 6 on log10(SPM); MAPD on SPM; median ratio satellite/*in situ*).

Sensor	Matchups	r^2	Slope	RMSD	Bias	MAPD (%)	Median ratio
Sentinel-3/OLCI	32	0.78	1.07	0.370	-0.243	45	0.62
Sentinel-2/MSI	11	0.88	1.18	0.433	-0.346	69	0.38

The satellite SPM follows the *in situ* SPM over two orders of magnitude, from about 3 g m^{-3} offshore to more than 100 g m^{-3} at MOW1 (r^2 = 0.78 for Sentinel-3 and 0.88 for Sentinel-2, on log10), but it underestimates it (Table 9, Figure 14): the bias is −0.24 for Sentinel-3 and −0.35 for Sentinel-2 (log10), i.e. a median ratio satellite/*in situ* of 0.62 and 0.38. The ratio varies strongly

between matchups: 11 of the 32 Sentinel-3 matchups agree within 20%, while 13 are below half of the *in situ* value. The relative underestimation is largest at the offshore stations W05 and W08 (median ratio 0.55 for Sentinel-3, 0.30 for Sentinel-2), where the *in situ* SPM is 3–11 g m^{-3}; at MOW1 the median ratio is 0.83 and 0.64.

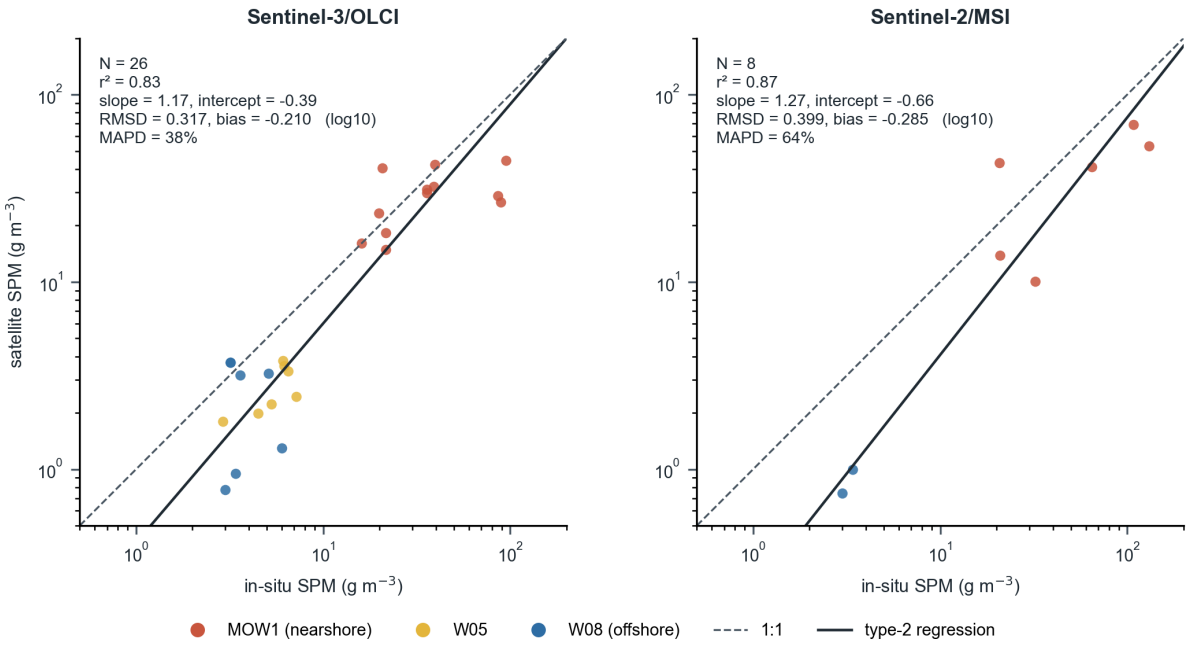


Figure 14: Satellite SPM against *in situ* SPM of the Belgian monitoring programme at MOW1 (nearshore), W05 and W08 (offshore), 2018–2023, within 3 hours: Sentinel-3/OLCI (left) and Sentinel-2/MSI (right). Dashed line: 1:1; solid line: type-2 regression; metrics on log10(SPM), MAPD on SPM.

On several of the eight days with matchups of both sensors, Sentinel-3 and Sentinel-2 give nearly the same ratio (e.g. 0.26 and 0.25, 0.28 and 0.29 at W08), so the two satellite products agree with each other where they both differ from the *in situ* value. The cause of the underestimation is under investigation; candidates are clouds or cloud shadows not detected by the pixel classification, the time difference between sampling and overpass in tidally variable waters, the representativeness of a single water sample for a 300 m or 60 m pixel, and the gravimetric SPM determination at low concentrations. The small number of matchups, in particular for Sentinel-2, limits these conclusions.

6.5 SEA SURFACE TEMPERATURE (SST)

The SST products are validated against the water temperature measured at 16 stations of the Meetnet Vlaamse Banken (Flemish Banks Monitoring Network, Flemish Government, Agency for Maritime and Coastal Services; https://meetnetvlaamsebanken.be) in the Belgian part of the North Sea (Figure 15), from April 2025 to March 2026. A matchup is the satellite SST in the 3×3 pixel box within 3 hours of the *in situ* measurement. At a given overpass the *in situ* temperatures of the stations differ by at most 0.6 °C, and the present extraction does not resolve the individual stations; the stations are therefore combined into one matchup per overpass, with the mean *in situ* temperature of the stations and the mean SST of the 3×3 box. This gives 55 matchups for Sentinel-3/SLSTR (Sentinel-3A and 3B) and 28 for Landsat-8/9/TIRS. The metrics of Table 6 are computed on SST in °C. The results are given in Table 10.

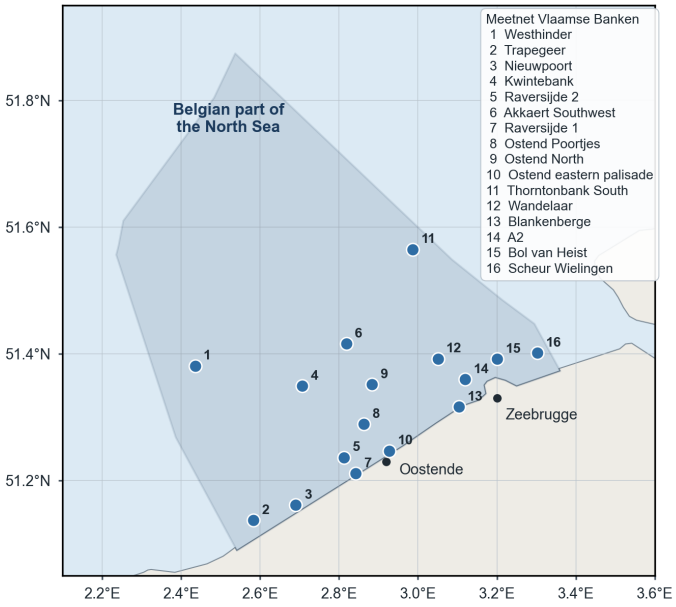


Figure 15: Stations of the Meetnet Vlaamse Banken in the Belgian part of the North Sea (shaded) used for the SST validation.

Four Landsat overpasses (22 and 30 April 2025, 18 June 2025 and 11 January 2026) are 3.3 to 5.1 °C colder than the *in situ* temperature, while all other overpasses differ by less than 2 °C. Such a cold offset is typical of thermal pixels affected by clouds, cloud edges or cloud shadows that are not removed by the pixel mask; these overpasses are removed, which leaves 24 Landsat matchups. With them, the Landsat RMSD would be 1.90 °C and the bias −0.72 °C.

Table 10: Validation of the SST against the Meetnet Vlaamse Banken, one matchup per overpass (metrics of Table 6 on SST in °C; Landsat without the four cloud-affected overpasses).

Sensor	Matchups	r^2	Slope	Intercept (°C)	RMSD (°C)	cRMSD (°C)	Bias (°C)
Sentinel-3/SLSTR	55	0.99	0.92	+0.97	0.72	0.64	-0.33
Landsat-8/9/TIRS	24	0.98	0.94	+0.72	0.85	0.84	-0.09

Both sensors agree closely with the *in situ* temperature over the seasonal range of 4 to 22 °C (Table 10, Figure 16): for Sentinel-3/SLSTR r^2 = 0.99, RMSD 0.72 °C and bias −0.33 °C; for Landsat-8/9/TIRS r^2 = 0.98, RMSD 0.85 °C and bias −0.09 °C. 45 of the 55 SLSTR matchups and 18 of the 24 Landsat matchups are within 1 °C of the *in situ* value. The warm bias of 1–2 K reported for the Landsat Collection-2 surface temperature over water (section 3.5) is not found here.

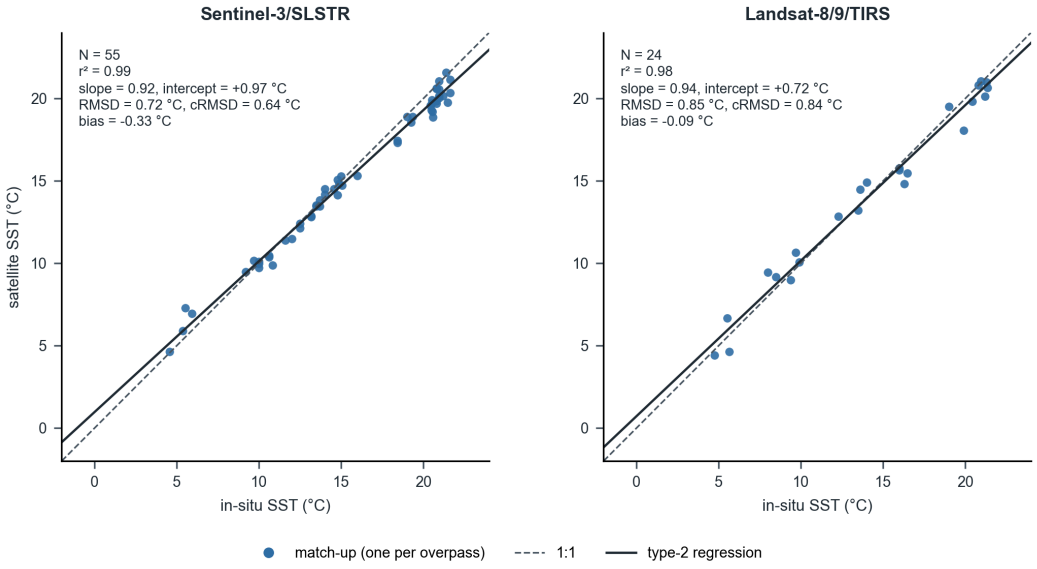


Figure 16: Satellite SST against the *in situ* SST of the Meetnet Vlaamse Banken, April 2025 – March 2026, within 3 hours, one matchup per overpass: Sentinel-3/SLSTR (left) and Landsat-8/9/TIRS without the four cloud-affected overpasses (right). Dashed line: 1:1; solid line: type-2 regression.

The type-2 slopes below one (0.92 for SLSTR, 0.94 for Landsat) reflect a seasonal pattern: the satellite SST is lower than the *in situ* temperature from April to September (mean difference −0.44 °C for SLSTR, −0.32 °C for Landsat) and higher from October to March (+0.56 °C and +0.38 °C). The satellites measure the skin temperature of the sea surface and the buoys the temperature below it, and the shallow nearshore waters warm faster in spring and summer and cool faster in autumn and winter than the deeper offshore waters, so the difference also depends on how well the satellite pixels and the stations represent the same water.

7 SYSTEM'S NOTICEABLE EVENTS, OUTAGES OR CHANGES

This section will document operational events affecting AQUASCOPE product quality or availability:

Date	Event Description	System Version	Impact	Resolution
TBD	Initial operational service	1.0	-	-

8 REFERENCES

Bailey, S. W., & Werdell, P. J. (2006). A multi-sensor approach for the on-orbit validation of ocean color satellite data products. *Remote Sensing of Environment*, 102(1-2), 12-23.

Brockmann, C., Doerffer, R., Peters, M., Stelzer, K., Embacher, S., & Ruescas, A. (2016). Evolution of the C2RCC neural network for Sentinel 2 and 3 for the retrieval of ocean colour products in normal and extreme optically complex waters. *Proceedings of the Living Planet Symposium 2016*, ESA SP-740, 54.

De Keukelaere, L., Sterckx, S., Adriaensen, S., Knaeps, E., Reusen, I., Giardino, C., Bresciani, M., Hunter, P., Neil, C., Van der Zande, D., & Vaiciute, D. (2018). Atmospheric correction of Landsat-8/OLI and Sentinel-2/MSI data using iCOR algorithm: validation for coastal and inland waters. *European Journal of Remote Sensing*, 51(1), 525-542.

Doerffer, R., & Schiller, H. (2007). The MERIS Case 2 water algorithm. *International Journal of Remote Sensing*, 28(3-4), 517-535.

He, K., Sun, J., & Tang, X. (2013). Guided image filtering. *IEEE Transactions on Pattern Analysis and Machine Intelligence*, 35(6), 1397-1409.

ISO (1999). *Water quality — Determination of turbidity*. ISO 7027:1999. International Organization for Standardization, Geneva.

Ke, G., Meng, Q., Finley, T., Wang, T., Chen, W., Ma, W., Ye, Q., & Liu, T.-Y. (2017). LightGBM: a highly efficient gradient boosting decision tree. *Advances in Neural Information Processing Systems 30 (NIPS 2017)*, 3146-3154.

Lavigne, H., Van der Zande, D., Ruddick, K., Dos Santos, J. C., Gohin, F., Brotas, V., & Kratzer, S. (2021). Quality-control tests for OC4, OC5 and NIR-red satellite chlorophyll-a algorithms applied to coastal waters. *Remote Sensing of Environment*, 255, 112237.

Luo, Y., Doxaran, D., Ruddick, K., Shen, F., Gentili, B., Yan, L., & Huang, H. (2018). Saturation of water reflectance in extremely turbid media based on field measurements, satellite data and bio-optical modelling. *Optics Express*, 26(8), 10435-10451.

Nechad, B., Ruddick, K. G., & Neukermans, G. (2009). Calibration and validation of a generic multisensor algorithm for mapping of turbidity in coastal waters. *Remote Sensing of the Ocean, Sea Ice, and Large Water Regions 2009*, SPIE Vol. 7473.

Nechad, B., Ruddick, K. G., & Park, Y. (2010). Calibration and validation of a generic multisensor algorithm for mapping of total suspended matter in turbid waters. *Remote Sensing of Environment*, 114(4), 854-866.

Novoa, S., Doxaran, D., Ody, A., Vanhellemont, Q., Lafon, V., Lubac, B., & Gernez, P. (2017). Atmospheric corrections and multi-conditional algorithm for multi-sensor remote sensing of suspended particulate matter in low-to-high turbidity levels coastal waters. *Remote Sensing*, 9(1), 61.

Pahlevan, N., Mangin, A., Balasubramanian, S. V., Smith, B., Alikas, K., Arai, K., ... & Warren, M. (2021). ACIX-Aqua: a global assessment of atmospheric correction methods for Landsat-8 and Sentinel-2 over lakes, rivers, and coastal waters. *Remote Sensing of Environment*, 258, 112366.

Ruddick, K. G., Brando, V. E., Corizzi, A., Dogliotti, A. I., Doxaran, D., Goyens, C., ... & Vanhellemont, Q. (2024). WATERHYPERNET: A prototype network of automated *in situ* measurements of hyperspectral water reflectance for satellite validation and water quality monitoring. *Frontiers in Remote Sensing*, 5, 1347520.

Steinmetz, F., Deschamps, P.-Y., & Ramon, D. (2011). Atmospheric correction in presence of sun glint: application to MERIS. *Optics Express*, 19(10), 9783-9800.

Tilstone, G., Moore, G., Sorensen, K., Doerffer, R., Röttgers, R., Ruddick, K. G., et al. (2003). REVAMP Regional Validation of MERIS Chlorophyll products in North Sea coastal waters: Protocols document. MAVT-2003, Frascati.

van der Linde, D. W. (1998). Protocol for the determination of total suspended matter in oceans and coastal zones. Technical Note I.98.182, JRC Ispra.

Van der Zande, D., Vanhellemont, Q., Stelzer, K., Lebreton, C., Dille, A., Cardoso Dos Santos, J., ... & Brockmann, C. (2023). Improving operational ocean color coverage using a merged atmospheric correction approach. *Remote Sensing of the Ocean, Sea Ice, Coastal Waters, and Large Water Regions 2023*, SPIE Vol. 12728.

Vanhellemont, Q. (2019). Adaptation of the dark spectrum fitting atmospheric correction for aquatic applications of the Landsat and Sentinel-2 archives. *Remote Sensing of Environment*, 225, 175-192.

Vanhellemont, Q. (2020a). Automated water surface temperature retrieval from Landsat 8/TIRS. *Remote Sensing of Environment*, 237, 111518.

Vanhellemont, Q. (2020b). Sensitivity analysis of the dark spectrum fitting atmospheric correction for metre- and decametre-scale satellite imagery using autonomous hyperspectral radiometry. *Optics Express*, 28(20), 29948-29965.

Vanhellemont, Q. (2021). S2/MSI detector geometry. Technical note, Royal Belgian Institute of Natural Sciences (RBINS), 29 June 2021 (unpublished).

Vanhellemont, Q., & Ruddick, K. (2021). Atmospheric correction of Sentinel-3/OLCI data for mapping of suspended particulate matter and chlorophyll-a concentration in Belgian turbid coastal waters. *Remote Sensing of Environment*, 256, 112284.

Vanhellemont, Q., Brewin, R. J., Bresnahan, P. J., & Cyronak, T. (2022). Validation of Landsat 8 high resolution sea surface temperature using surfers. *Estuarine, Coastal and Shelf Science*, 265, 107650.

Vansteenwegen, D., Ruddick, K., Cattrijsse, A., Vanhellemont, Q., & Beck, M. (2019). The pan-and-tilt hyperspectral radiometer system (PANTHYR) for autonomous satellite validation measurements: prototype design and testing. *Remote Sensing*, 11(11), 1360.

Wevers, J., Müller, D., Scholze, J., Kirches, G., Quast, R., & Brockmann, C. (2021). IdePix for Sentinel-2 MSI Algorithm Theoretical Basis Document (version 1.0). *Zenodo*, https://doi.org/10.5281/zenodo.5788067.

Zibordi, G., Mélin, F., Berthon, J.-F., Holben, B., Slutsker, I., Giles, D., D'Alimonte, D., Vandemark, D., Feng, H., Schuster, G., Fabbri, B. E., Kaitala, S., & Seppälä, J. (2009). AERONET-OC: a network for the validation of ocean color primary products. *Journal of Atmospheric and Oceanic Technology*, 26(8), 1634-1651.